ENHANCED DIPOLE STRENGTH BELOW PARTICLE THRESHOLD

R. Schwengner[1], G. Rusev[1,2], N. Benouaret[1,3], R. Beyer[1], M. Erhard[1], E. Grosse[1], A. R. Junghans[1], K. Kosev[1], C. Nair[1], K. D. Schilling[1], A. Wagner[1], S. Q. Zhang[1,4], F. Dönau[1], S. Frauendorf[1,5], N. Tsoneva[6], H. Lenske[6]

[1] *Institut für Strahlenphysik, Forschungszentrum Dresden-Rossendorf, 01314 Dresden, Germany*
[2] *Dept. of Physics, Duke University, and Triangle Universities Nuclear Laboratory, Durham, NC 27708*
[3] *Faculté de Physique, Université des Sciences et de la Technologie d'Alger, 16111 Bab-Ezzouar, Algerie*
[4] *Beijing University, Beijing 100871, China*
[5] *Department of Physics, University of Notre Dame, Notre Dame, IN 46556*
[6] *Institut für Theoretische Physik, Universität Gießen, 35392 Gießen, Germany*

- Photon-scattering experiments at ELBE
- Data analysis and results
- Model predictions

Supported by Deutsche Forschungsgemeinschaft

Dipole strength close to the particle-separation energy

- Modelling of astrophysical processes:
  - (γ,n) reaction rates in the p-process.
  - (n,γ) reaction rates in the s-process.
- Studies for future nuclear-fuel cycles:
  - improved experimental and theoretical description of (n,γ) reactions.
- Open problems:
  - precise knowledge of the dipole strength on the low-energy tail of the Giant Dipole Resonance below the particle thresholds.
  - properties of the dipole strength functions at varying proton and neutron numbers: shell effects, deformation etc.

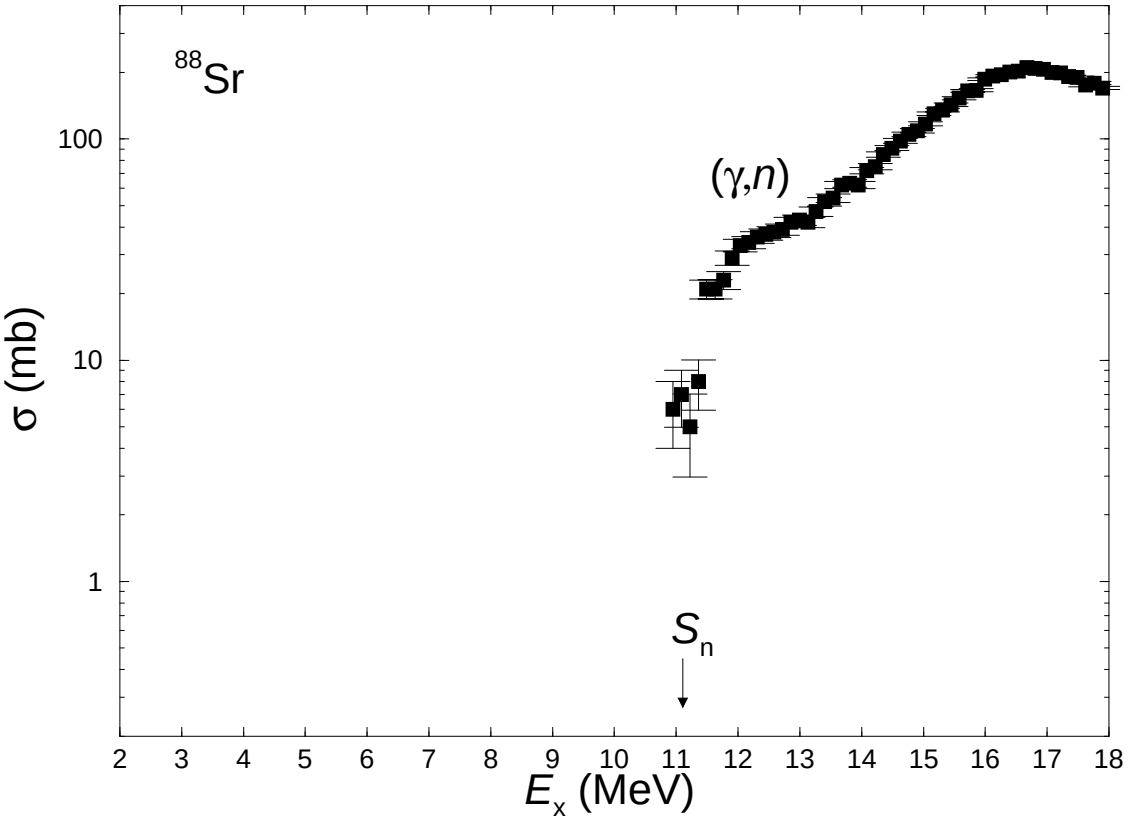

Dipole strength close to the particle-separation energy

- Modelling of astrophysical processes:
  - (γ,n) reaction rates in the p-process.
  - (n,γ) reaction rates in the s-process.
- Studies for future nuclear-fuel cycles:
  - improved experimental and theoretical description of (n,γ) reactions.
- Open problems:
  - precise knowledge of the dipole strength on the low-energy tail of the Giant Dipole Resonance below the particle thresholds.
  - properties of the dipole strength functions at varying proton and neutron numbers: shell effects, deformation etc.

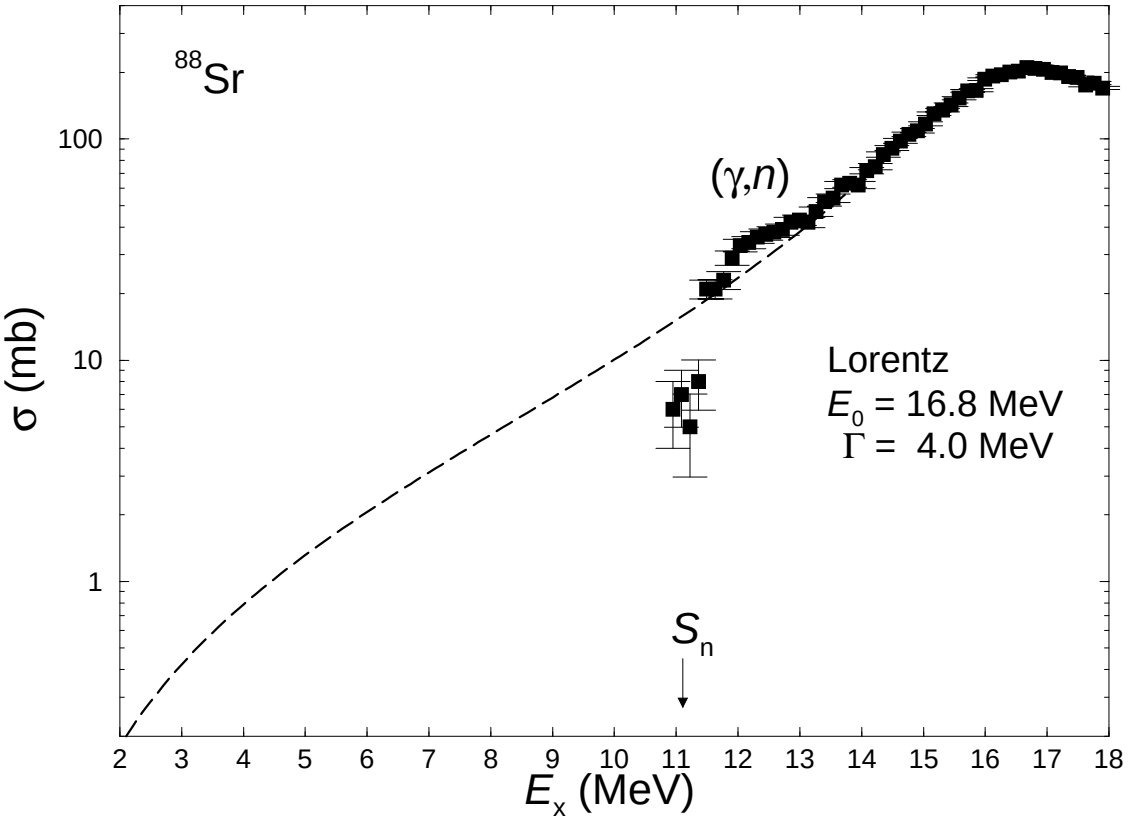

Dipole strength close to the particle-separation energy

- Modelling of astrophysical processes:
  - (γ,n) reaction rates in the p-process.
  - (n,γ) reaction rates in the s-process.
- Studies for future nuclear-fuel cycles:
  - improved experimental and theoretical description of (n,γ) reactions.
- Open problems:
  - precise knowledge of the dipole strength on the low-energy tail of the Giant Dipole Resonance below the particle thresholds.
  - properties of the dipole strength functions at varying proton and neutron numbers: shell effects, deformation etc.

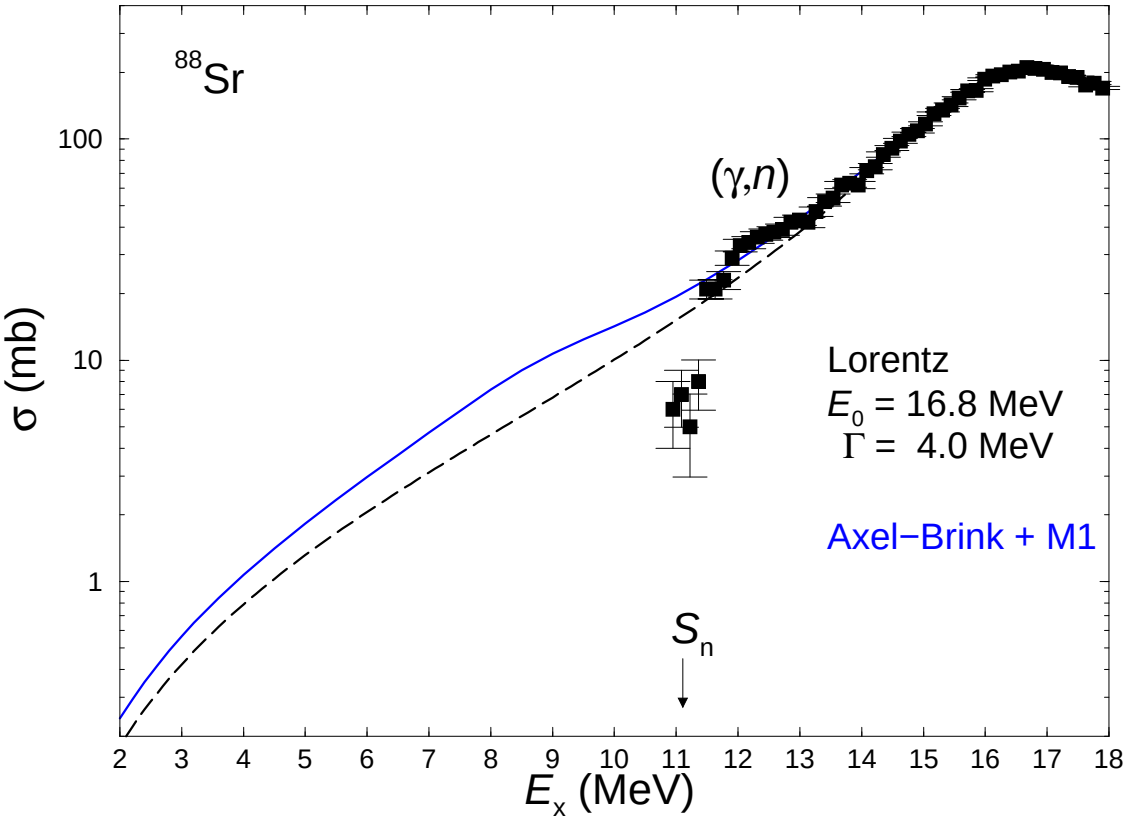

Dipole strength close to the particle-separation energy

- Modelling of astrophysical processes:
  - (γ,n) reaction rates in the p-process.
  - (n,γ) reaction rates in the s-process.
- Studies for future nuclear-fuel cycles:
  - improved experimental and theoretical description of (n,γ) reactions.
- Open problems:
  - precise knowledge of the dipole strength on the low-energy tail of the Giant Dipole Resonance below the particle thresholds.
  - properties of the dipole strength functions at varying proton and neutron numbers: shell effects, deformation etc.

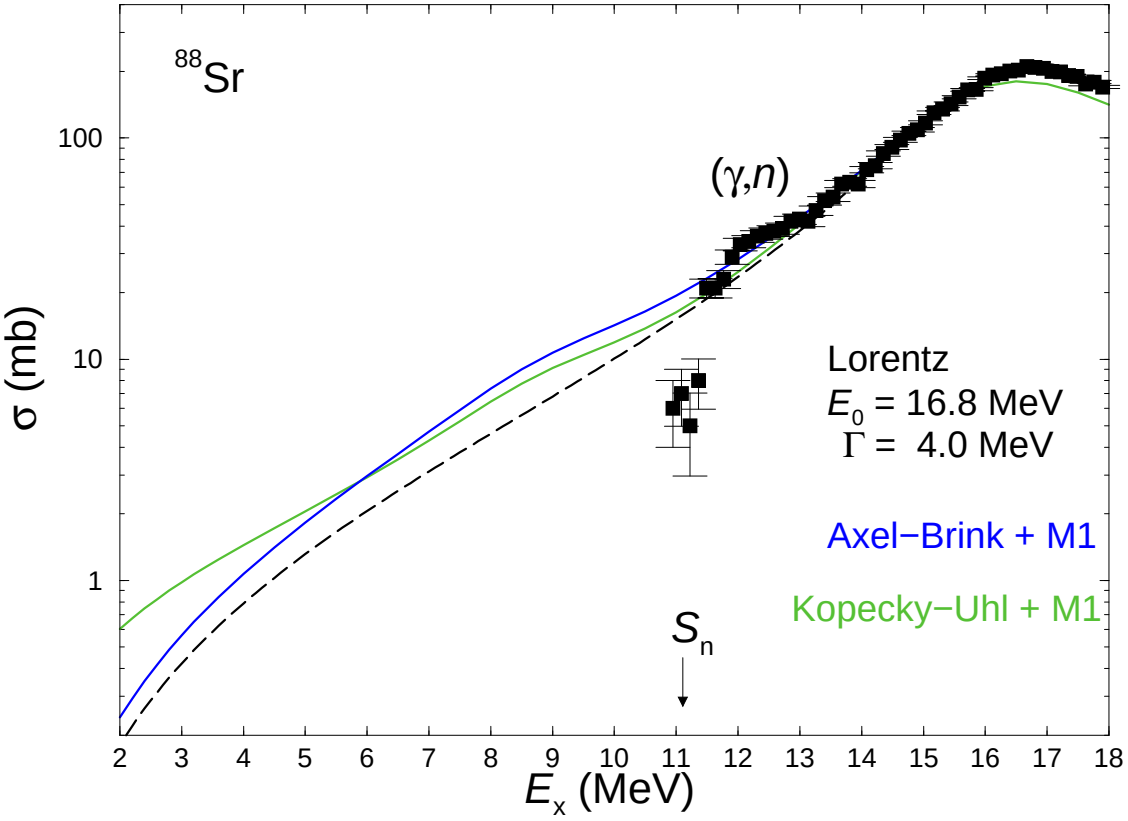

Dipole strength close to the particle-separation energy

- Modelling of astrophysical processes:
  - (γ,n) reaction rates in the p-process.
  - (n,γ) reaction rates in the s-process.
- Studies for future nuclear-fuel cycles:
  - improved experimental and theoretical description of (n,γ) reactions.
- Open problems:
  - precise knowledge of the dipole strength on the low-energy tail of the Giant Dipole Resonance below the particle thresholds.
  - properties of the dipole strength functions at varying proton and neutron numbers: shell effects, deformation etc.

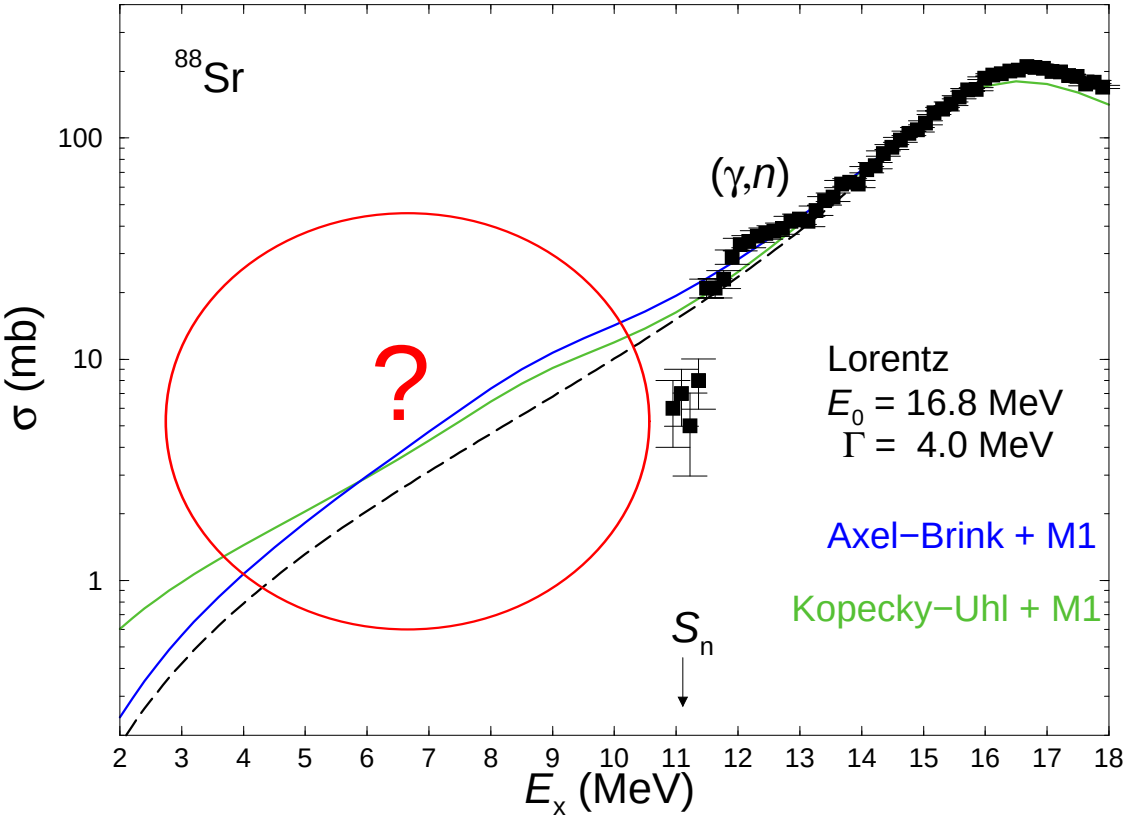

Electron Linear accelerator of high Brilliance and low Emittance

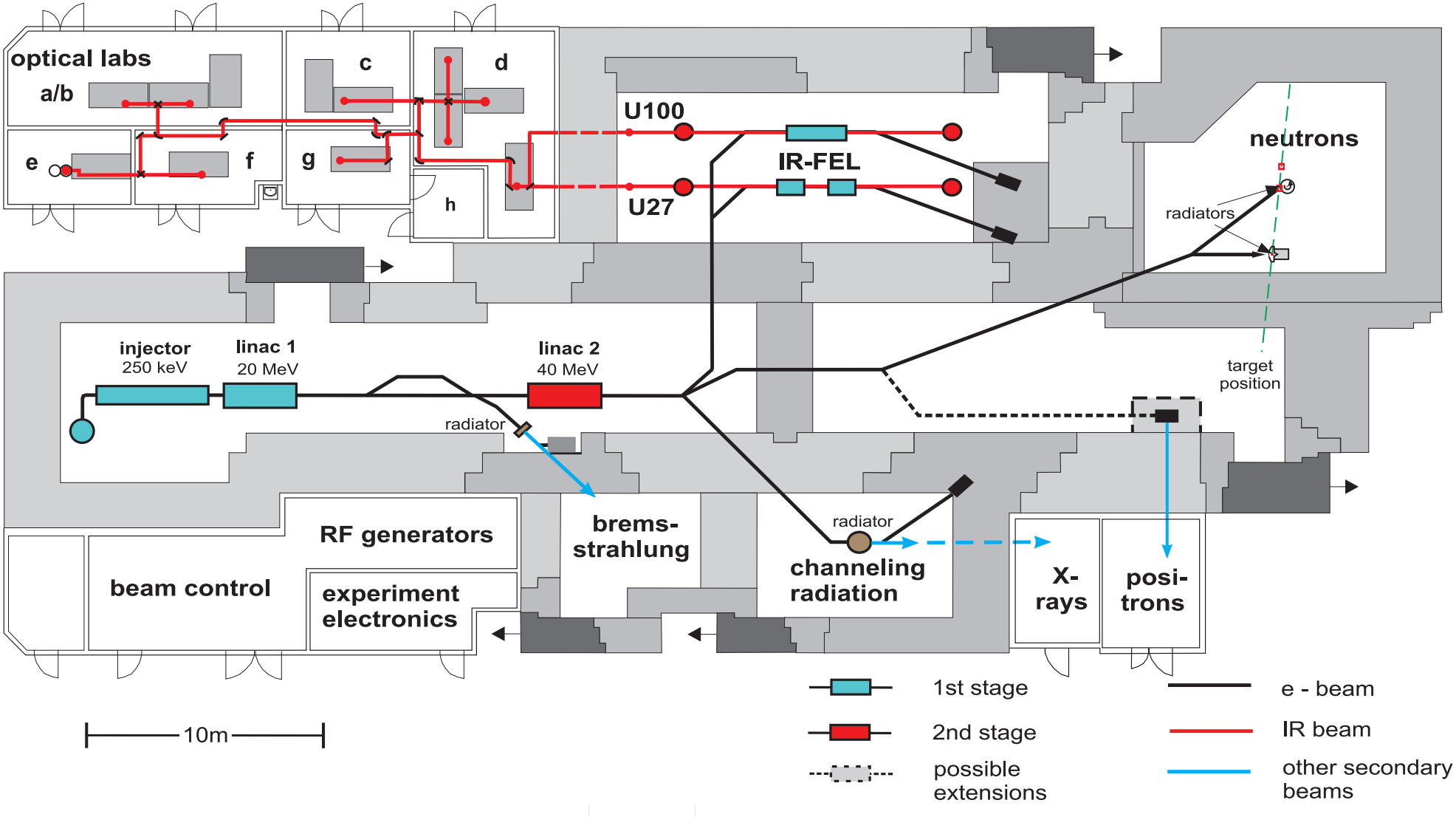

The bremsstrahlung facility at the electron accelerator ELBE

Accelerator parameters:

- Maximum electron energy:
  $\approx$ 18 MeV
- Maximum average current:
  $\approx$ 0.8 mA
- Micro-pulse rate:
  13 MHz
- Micro-pulse length:
  $\approx$ 5 ps

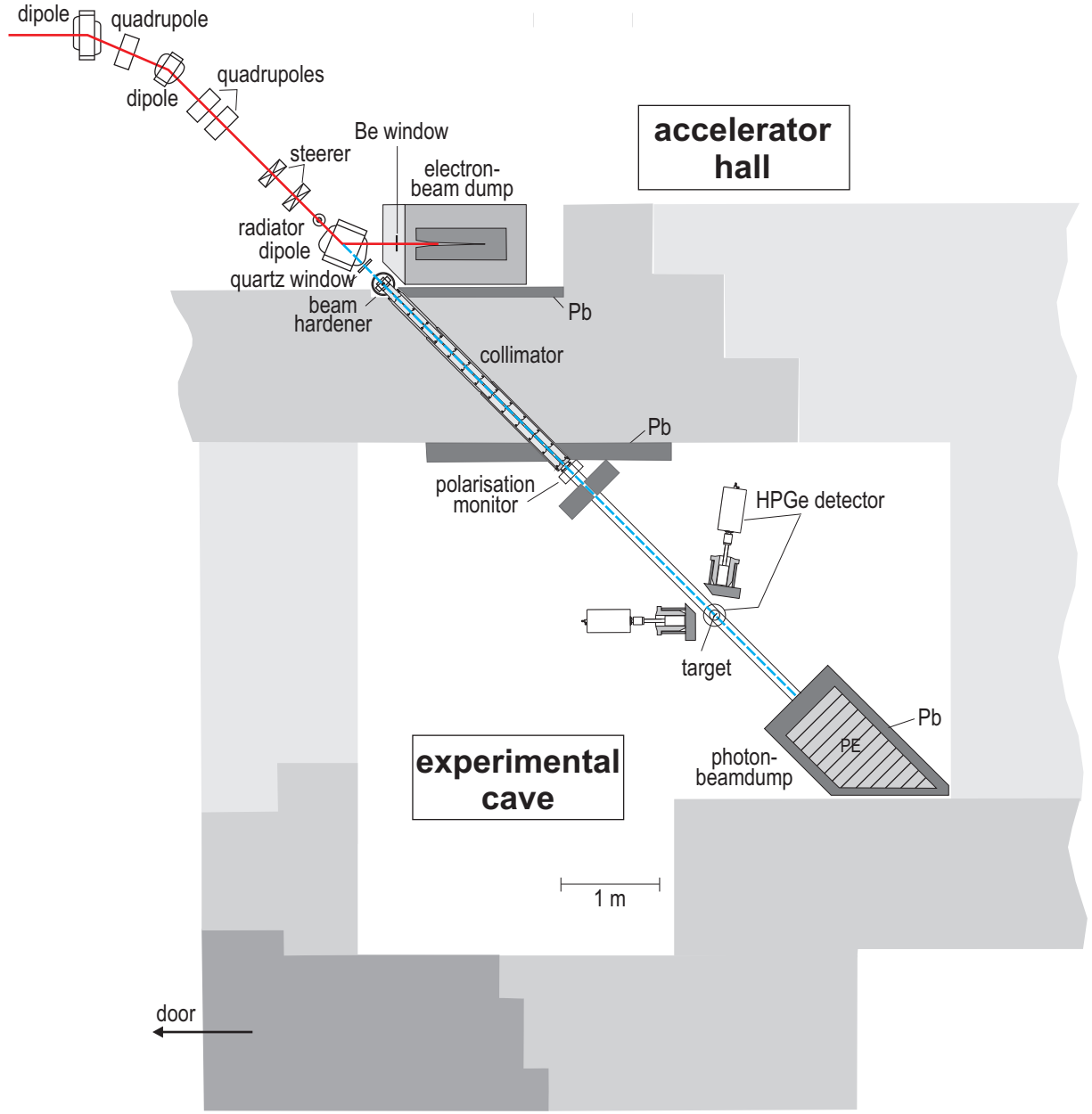

R.S. et al., NIM A 555 (2005) 211

Detector setup

Nuclides under investigation in photon-scattering experiments

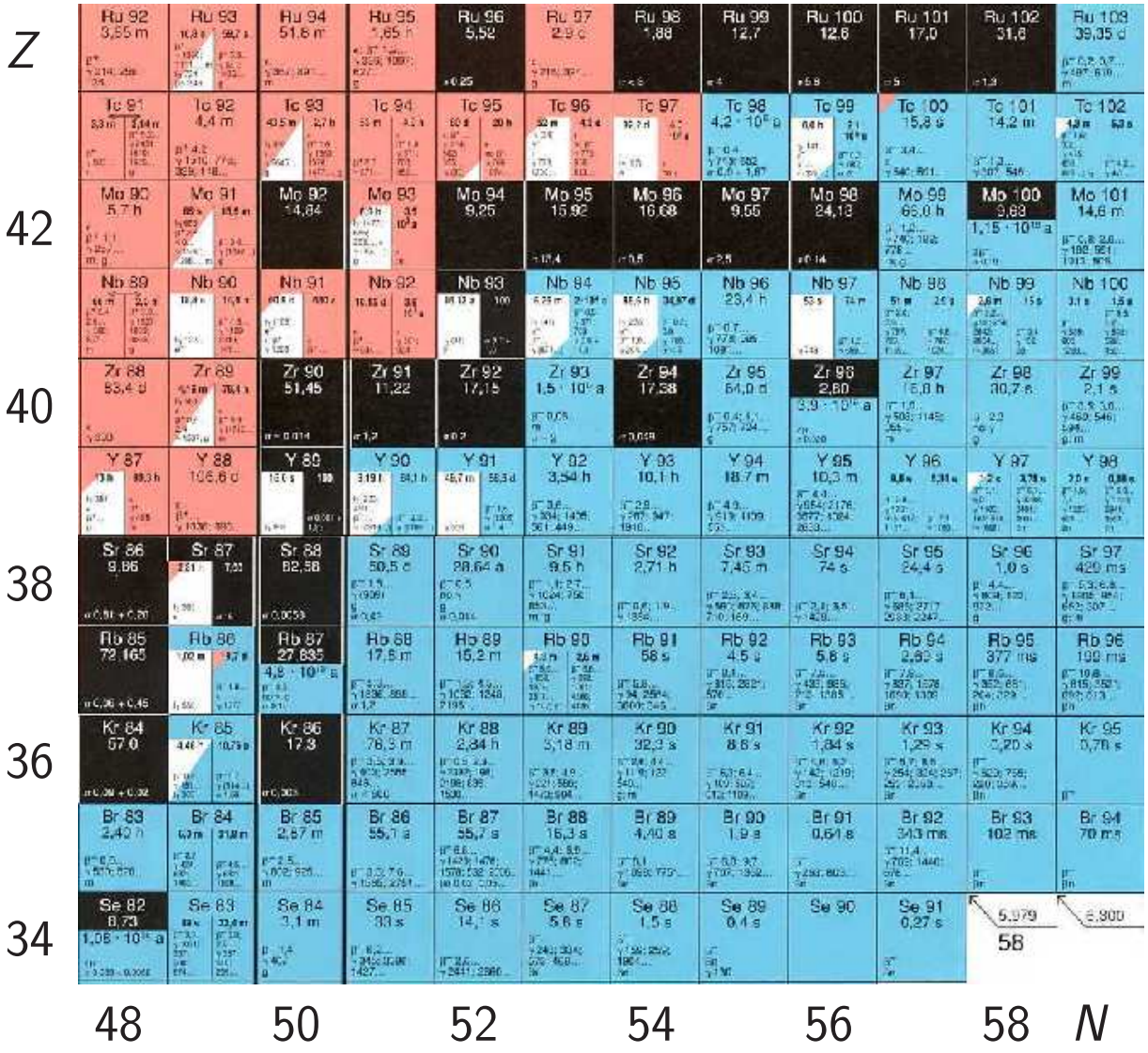

nuclide	S_n MeV	E_e^{kin} (MeV) ELBE
^{92}Mo	12.7	6.0[a], 13.2[b,c,d]
^{94}Mo	9.7	13.2[d]
^{96}Mo	9.2	13.2[d]
^{98}Mo	8.6	(3.3, 3.8)[a,e], (8.5, 13.2)[b,c,d]
^{100}Mo	8.3	(3.2, 3.4, 3.8)[a], (7.8, 13.2)[b,c,d]
^{90}Zr	12.0	(7.0, 9.0, 13.2) [f]
^{89}Y	11.5	7.0, (9.5, 13.2) [g]
^{88}Sr	11.1	6.8, (9.0, 13.2, 16.0)[h]
^{87}Rb	9.9	4.0, 13.2
^{86}Kr	9.9	11.2

[a] G. Rusev et al., PRC 73 (2006) 044308
[b] R. Schwengner et al., NPA 788 (2007) 331c
[c] G. Rusev et al., PRC 77 (2008) 064321
[d] A. Wagner et al., JPG 35 (2008) 014035
[e] G. Rusev et al., PRL 95 (2005) 062501
[f] R. Schwengner et al., PRC 78 (2008) 064314
[g] N. Benouaret et al., PRC 79 (2009) 014303
[h] R. Schwengner et al., PRC 76 (2007) 034321

Problem of feeding and branching

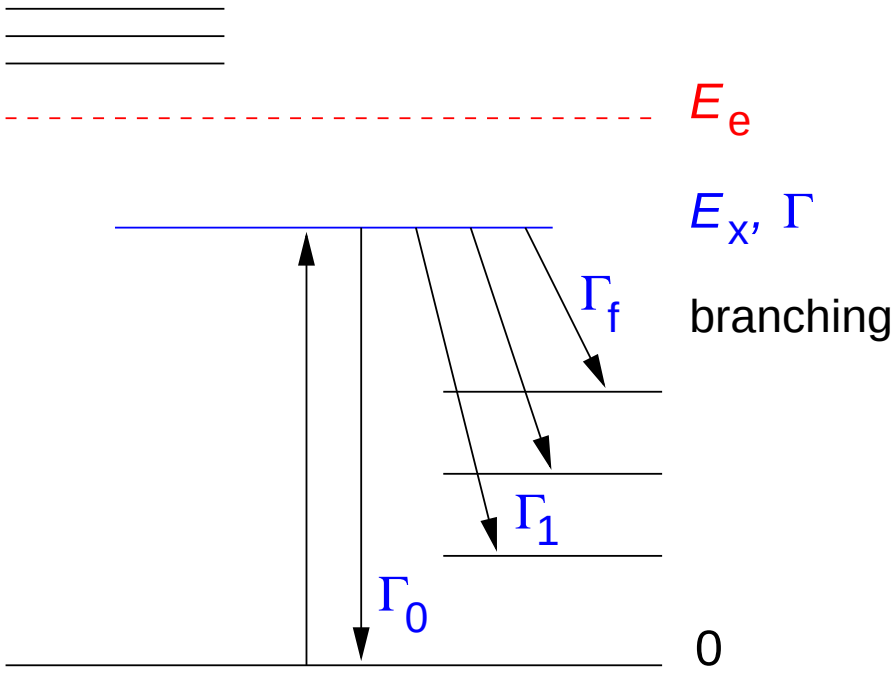

Measured intensity of a γ transition:

$$I_\gamma(E_\gamma, \Theta) = I_s(E_x)\, \Phi_\gamma(E_x)\, \epsilon(E_\gamma)\, N_{at}\, W(\Theta)\, \Delta\Omega$$

Integrated scattering cross section:

$$I_s = \int \sigma_{\gamma\gamma}\, dE = \frac{2J_x + 1}{2J_0 + 1} \left(\frac{\pi\hbar c}{E_x}\right)^2 \frac{\Gamma_0}{\Gamma}\, \Gamma_0$$

Absorption cross section:

$$\sigma_\gamma = \sigma_{\gamma\gamma} \left(\frac{\Gamma_0}{\Gamma}\right)^{-1}$$

E1 strength:

$$B(E1) \sim \Gamma_0 / E_\gamma^3$$

Problem of feeding and branching

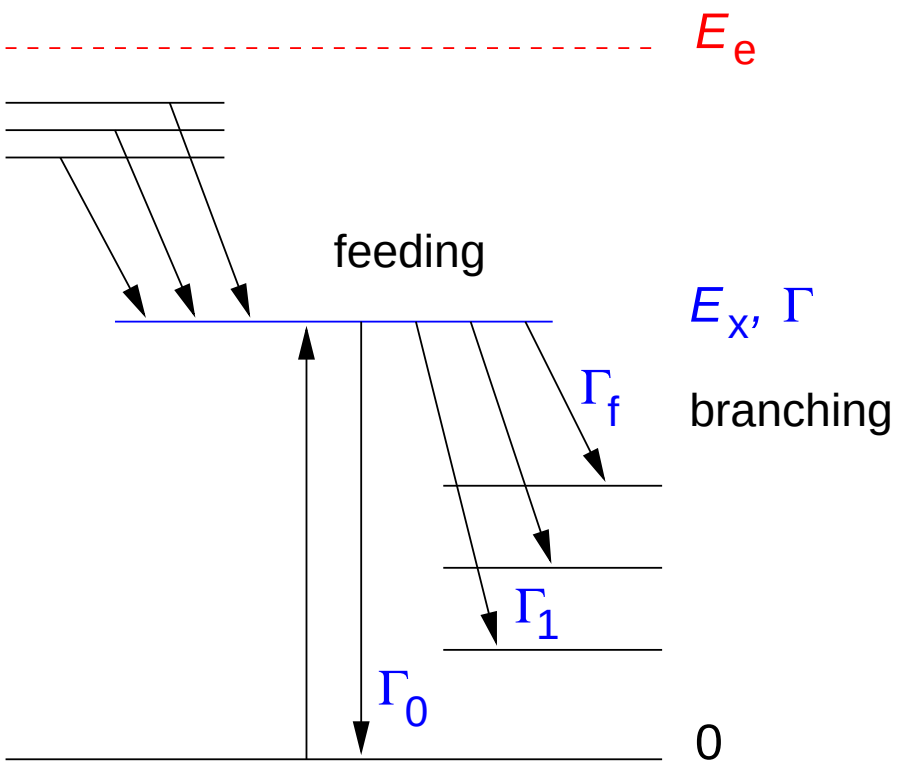

Measured intensity of a γ transition:

$$I_\gamma(E_\gamma, \Theta) > I_s(E_x)\, \Phi_\gamma(E_x)\, \epsilon(E_\gamma)\, N_{at}\, W(\Theta)\, \Delta\Omega$$

Integrated scattering cross section:

$$I_s = \int \sigma_{\gamma\gamma}\, dE = \frac{2J_x + 1}{2J_0 + 1} \left(\frac{\pi\hbar c}{E_x}\right)^2 \frac{\Gamma_0}{\Gamma}\, \Gamma_0$$

Absorption cross section:

$$\sigma_\gamma = \sigma_{\gamma\gamma} \left(\frac{\Gamma_0}{\Gamma}\right)^{-1}$$

E1 strength:

$$B(E1) \sim \Gamma_0 / E_\gamma^3$$

Production of linearly polarised off-axis bremsstrahlung

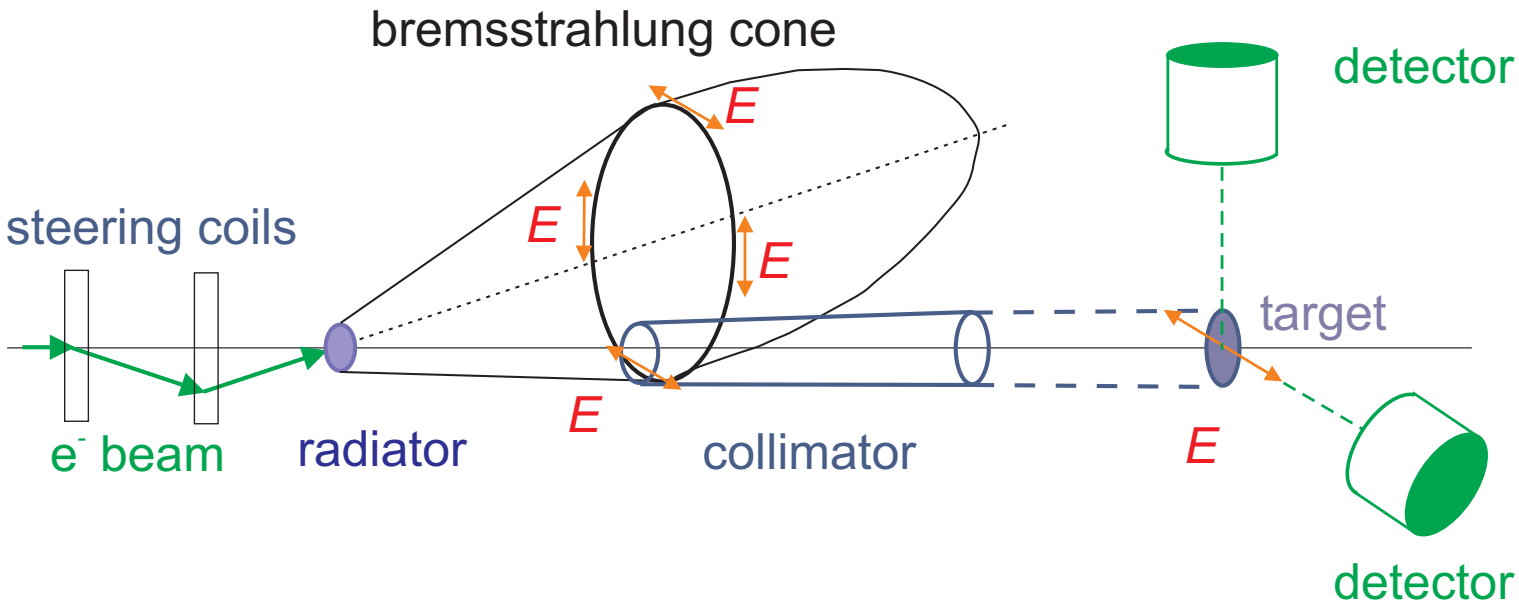

Measurement with polarised photons

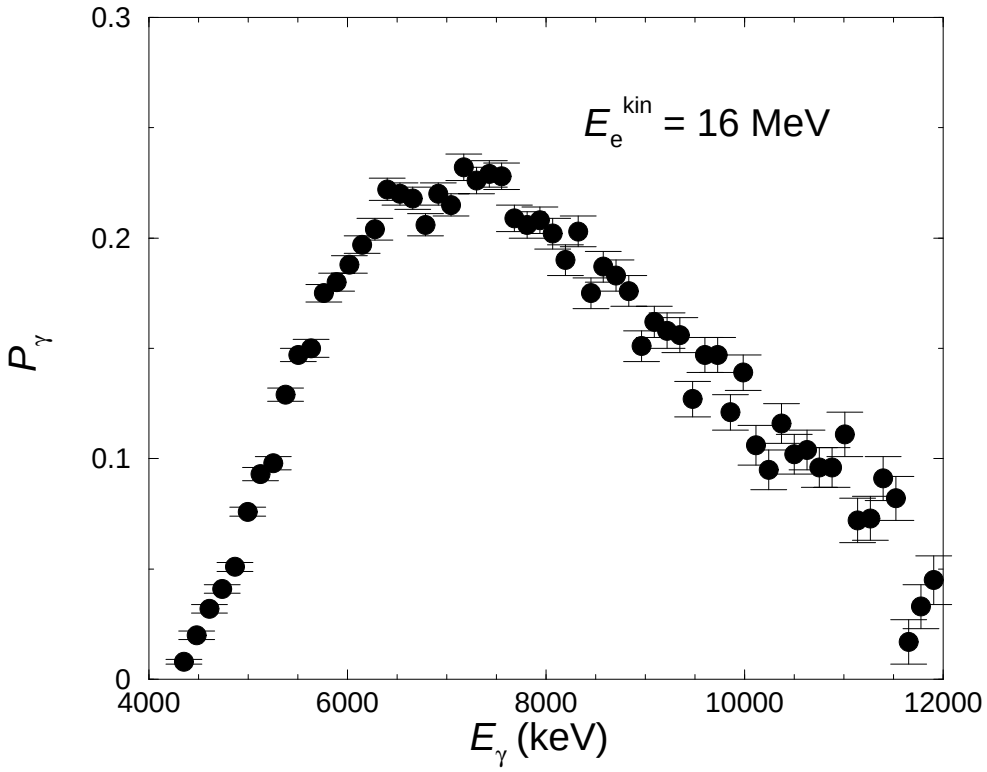

Degree of polarisation deduced from spectra of protons emitted in the disintegration of deuterons $d(\vec{\gamma}, p)n$.

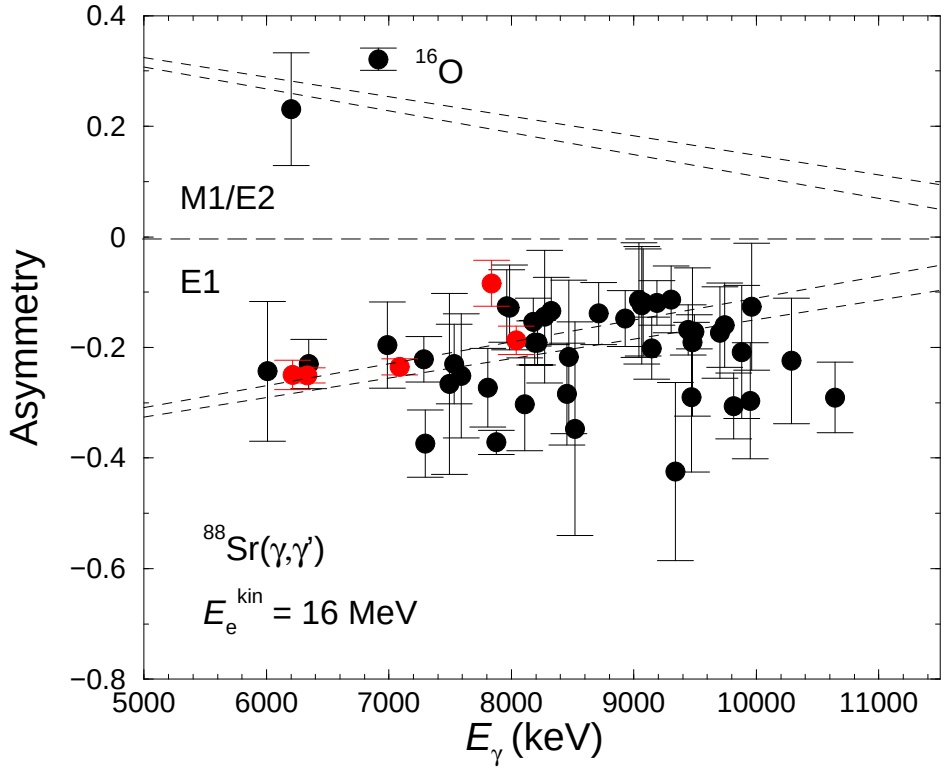

Azimuthal asymmetries $(N_{\gamma\parallel} - N_{\gamma\perp})/(N_{\gamma\parallel} + N_{\gamma\perp})$ of intensities of γ rays in ^{88}Sr.

Unresolved strength in the continuum

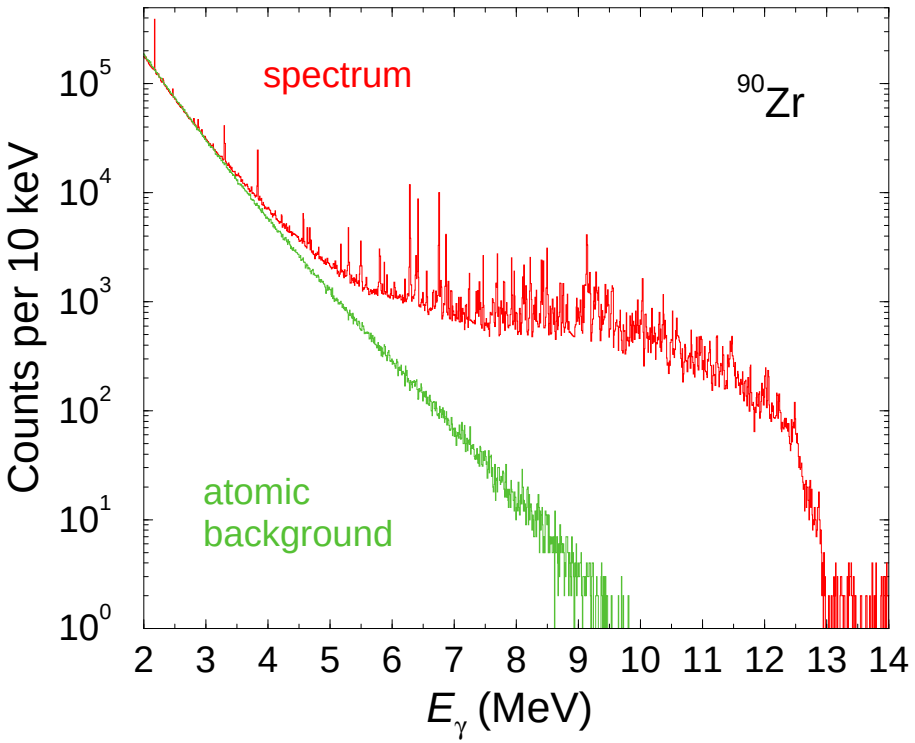

Experimental spectrum of ^{90}Zr (corrected for room background, detector response, efficiency, measuring time) and simulated spectrum of atomic background.

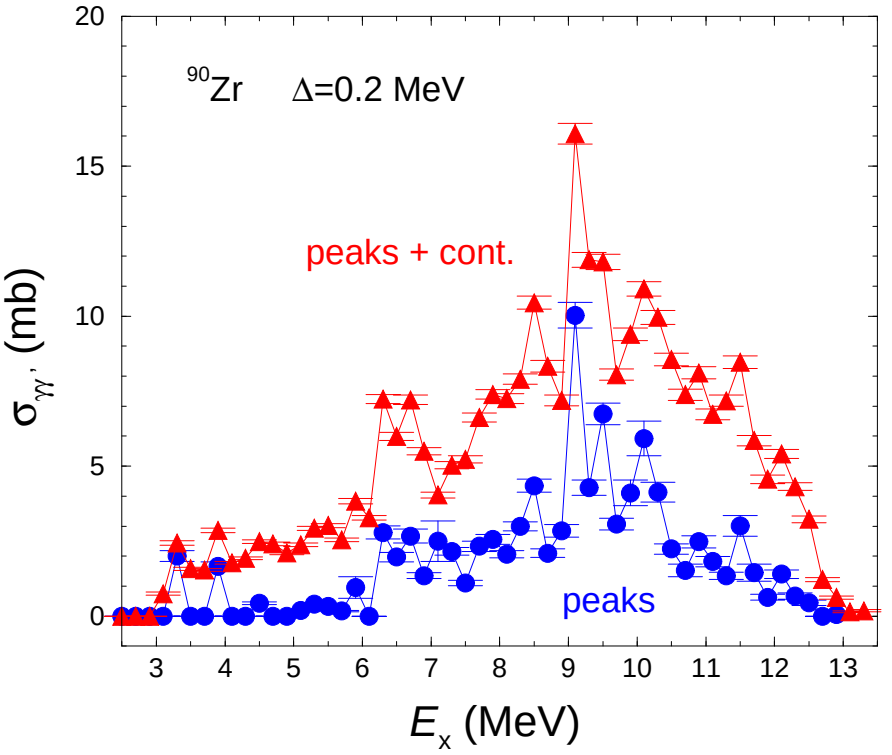

Scattering cross sections in ^{90}Zr averaged over energy bins of 0.2 MeV, not corrected for branching, derived from the difference of the experimental spectrum and the atomic background (triangles) and from the resolved peaks only (circles).

Level densities in Mo isotopes

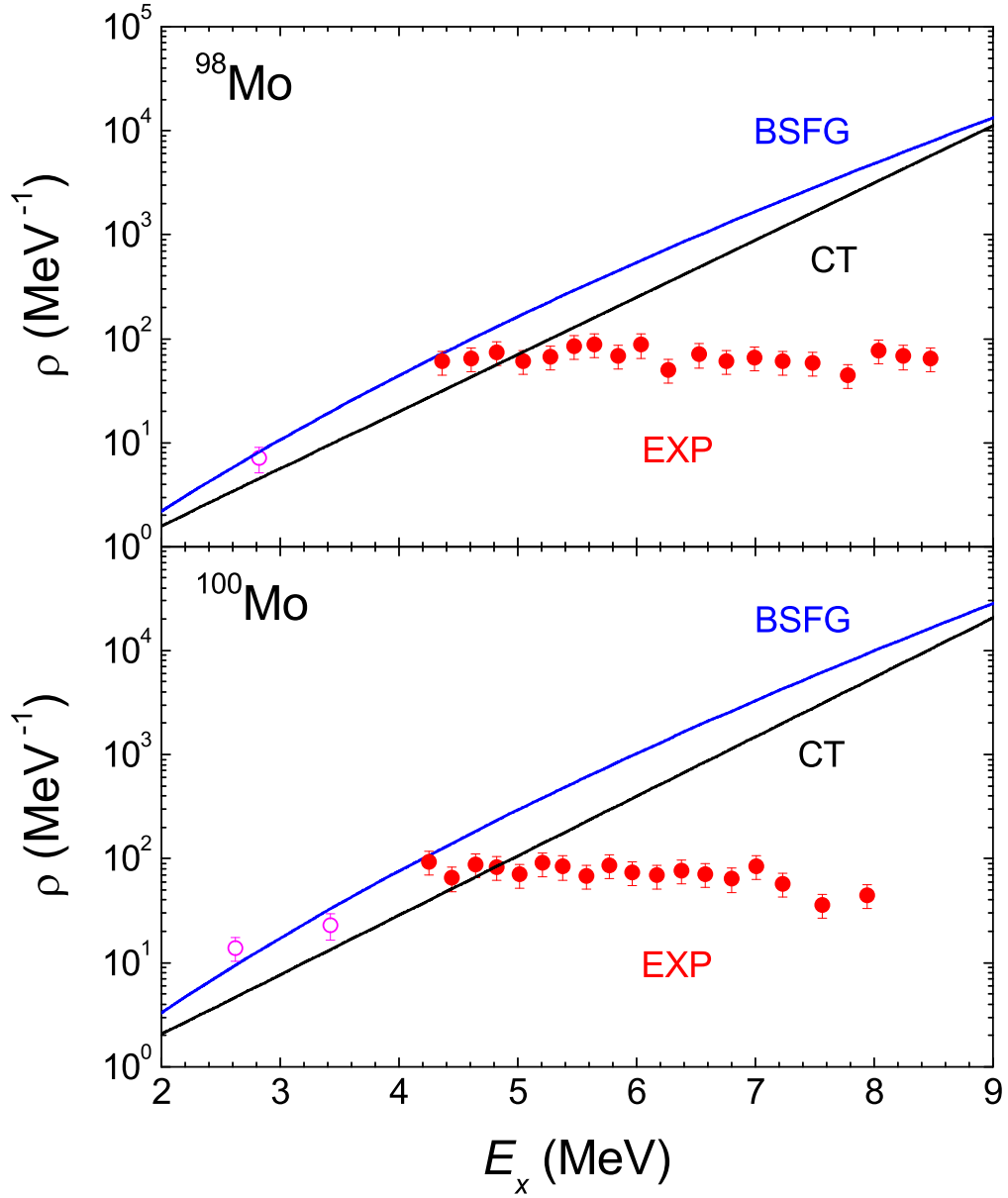

Experiment at $E_e^{kin} = 3.8$ MeV

Experiment at $E_e^{kin} = 13.2$ MeV

Back-shifted Fermi gas (BSFG) model

Constant-temperature (CT) approximation

Simulations of γ-ray cascades

Monte Carlo simulations of γ-ray cascades from groups of levels in 100 keV bins (G. Rusev, dissertation)

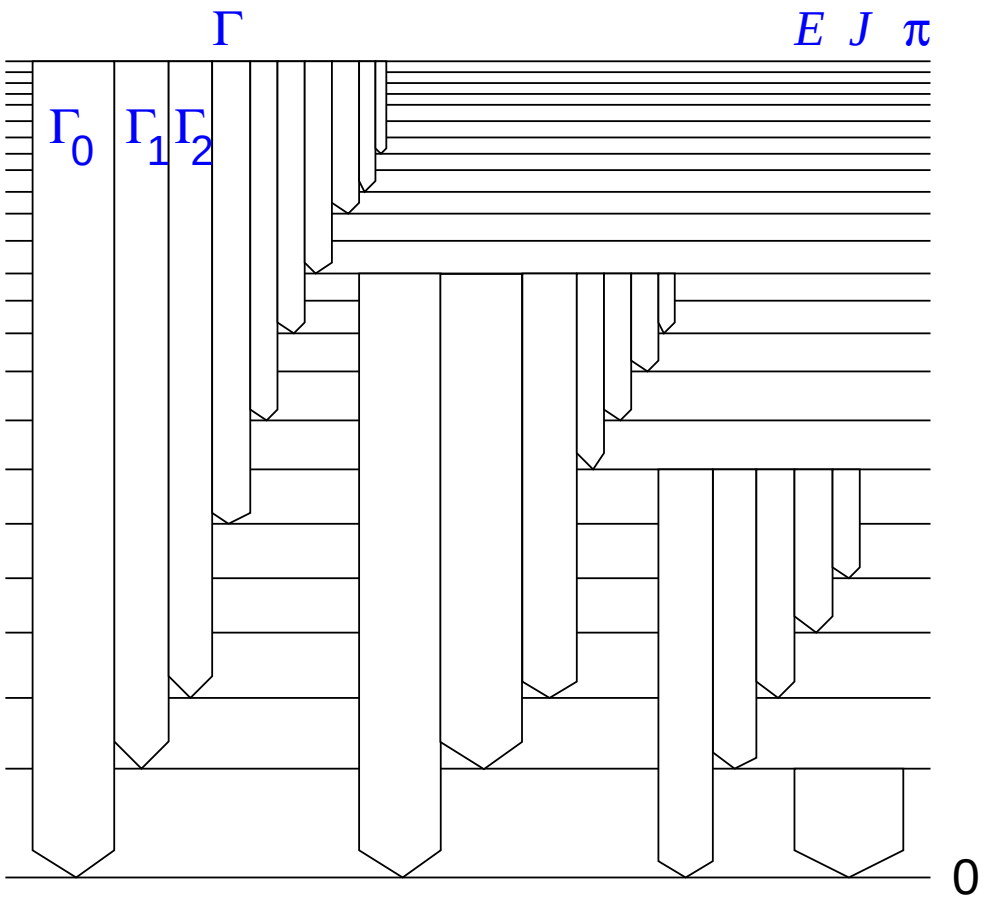

⇒ Level scheme of $J = 0, 1, 2$ states constructed by using:
- Backshifted Fermi-Gas Model with level-density parameters from T. v. Egidy, D. Bucurescu, PRC 72 (2005) 044311
- Wigner level-spacing distributions

⇒ Partial decay widths calculated by using:
- Photon strength functions approximated by Lorentz curves (www-nds.iaea.org/RIPL-2).
  $E1$: parameters from fit to (γ,n) data
  $M1$: global parametrisation of spin-flip resonances
  $E2$: global parametrisation of isoscalar resonances
- Porter-Thomas distributions of decay widths.

⇒ Feeding intensities subtracted and intensities of g.s. transitions corrected with calculated branching ratios Γ_0/Γ.

Simulations of γ-ray cascades

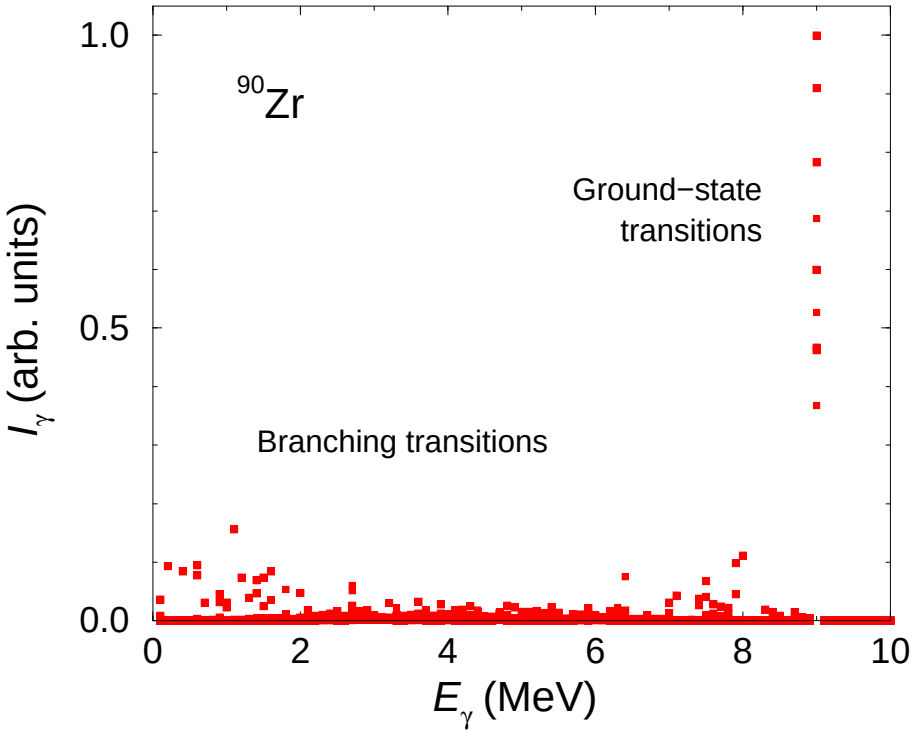

Simulated intensity distribution of transitions depopulating levels in a 100 keV bin around 9 MeV.
$\Rightarrow$ *Subtraction of intensities of branching transitions.*

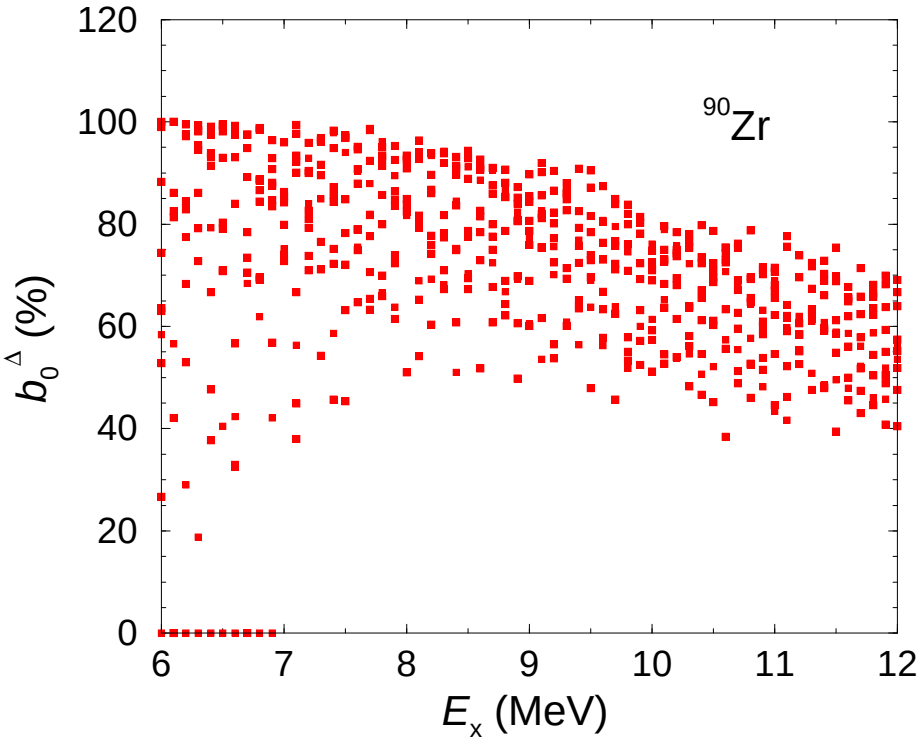

Distribution of branching ratios $b_0 = \Gamma_0/\Gamma$ versus the excitation energy as obtained from the simulations of γ-ray cascades for ^{90}Zr.
$\Rightarrow$ *Estimate of Γ_0 and σ_γ.*

Test of simulated branching ratios - Measurement at HIγS

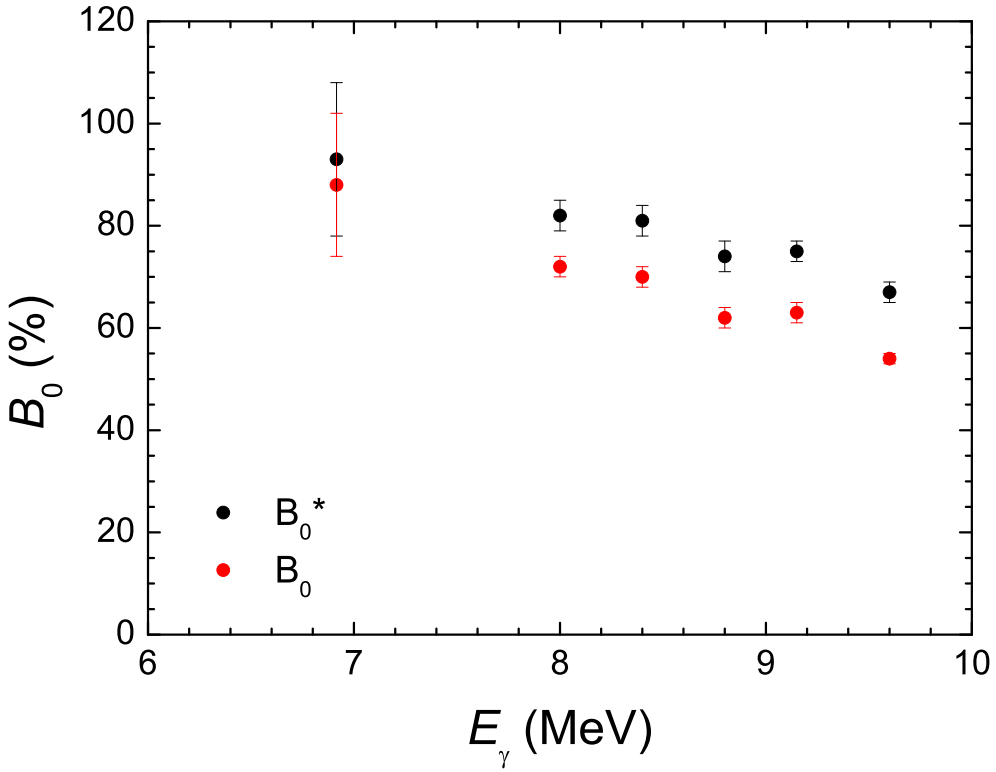

Measurement with monochromatic photons at HIγS ($\Delta E \approx 200$ keV).
Black: Population of 0_2^+ neglected.
Red: Assumption that $b_{0_2^+} = b_{2_1^+}$.
G. Rusev, A.P. Tonchev et al.

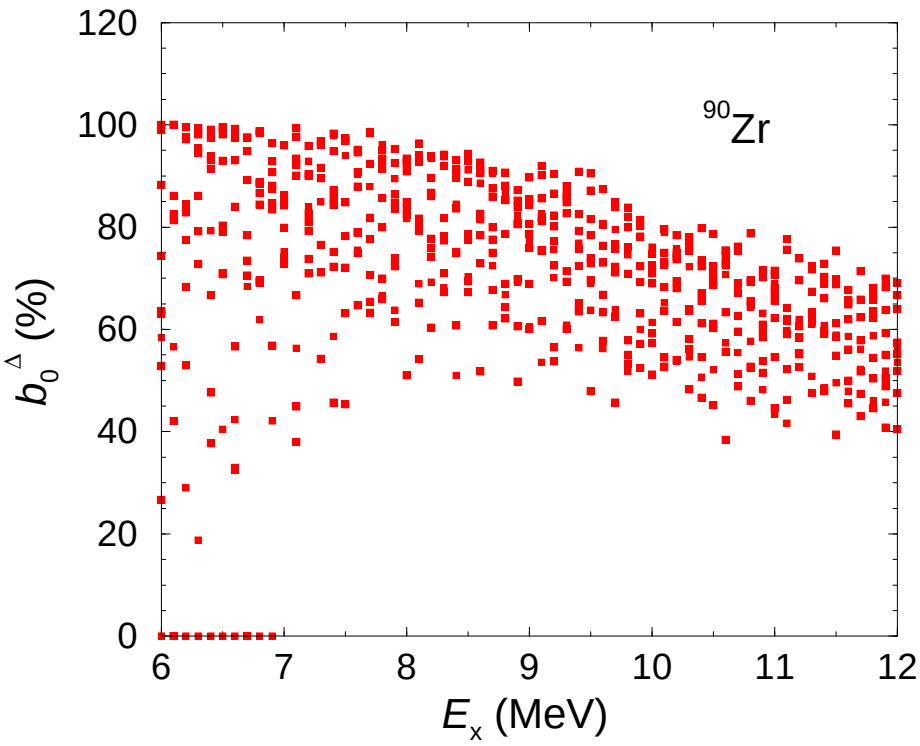

Distribution of branching ratios $b_0 = \Gamma_0/\Gamma$ versus the excitation energy as obtained from the simulations of γ-ray cascades for ^{90}Zr.

Test of simulated branching ratios - Measurements at HIγS

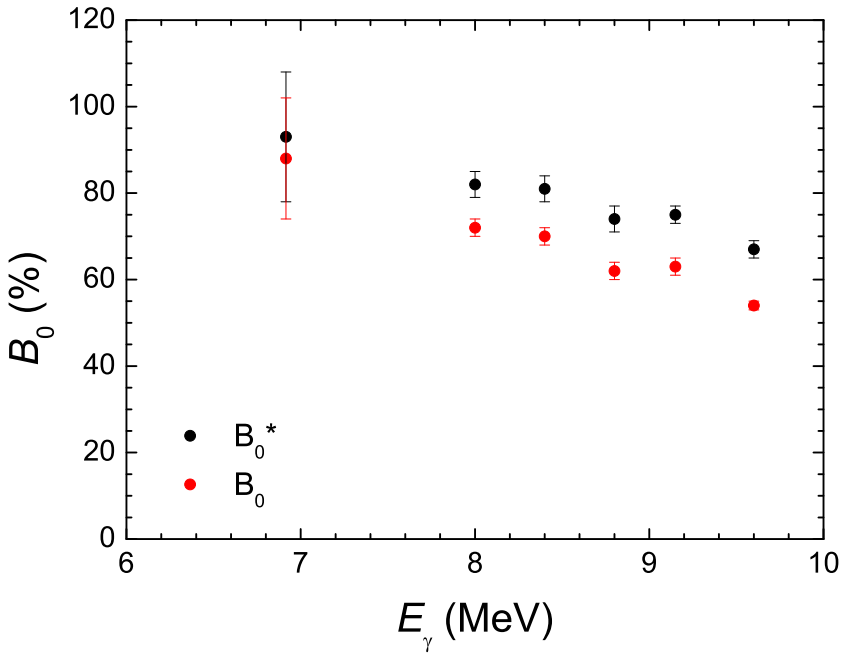

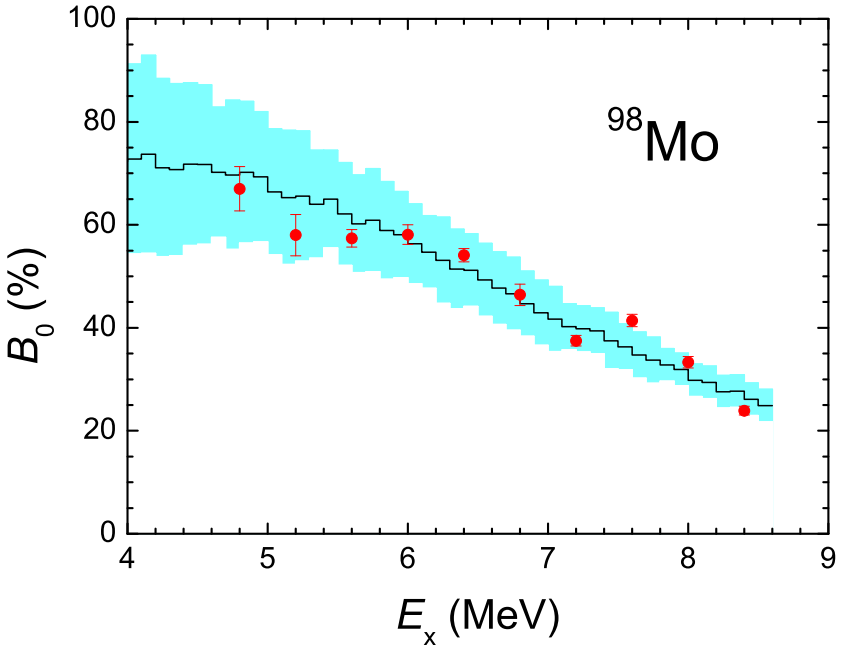

Measurements with monochromatic photons at HIγS ($\Delta E \approx 200$ keV).
Black: Population of 0_2^+ neglected.
Red: Assumption that $b_{0_2^+} = b_{2_1^+}$.
G. Rusev, A.P. Tonchev et al.

Branching ratios $b_0 = \Gamma_0/\Gamma$ versus the excitation energy as obtained from simulations of γ-ray cascades (black line - average) and from measurements with monochromatic photons at HIγS for ^{98}Mo (red circles).

Absorption cross section in ^{89}Y

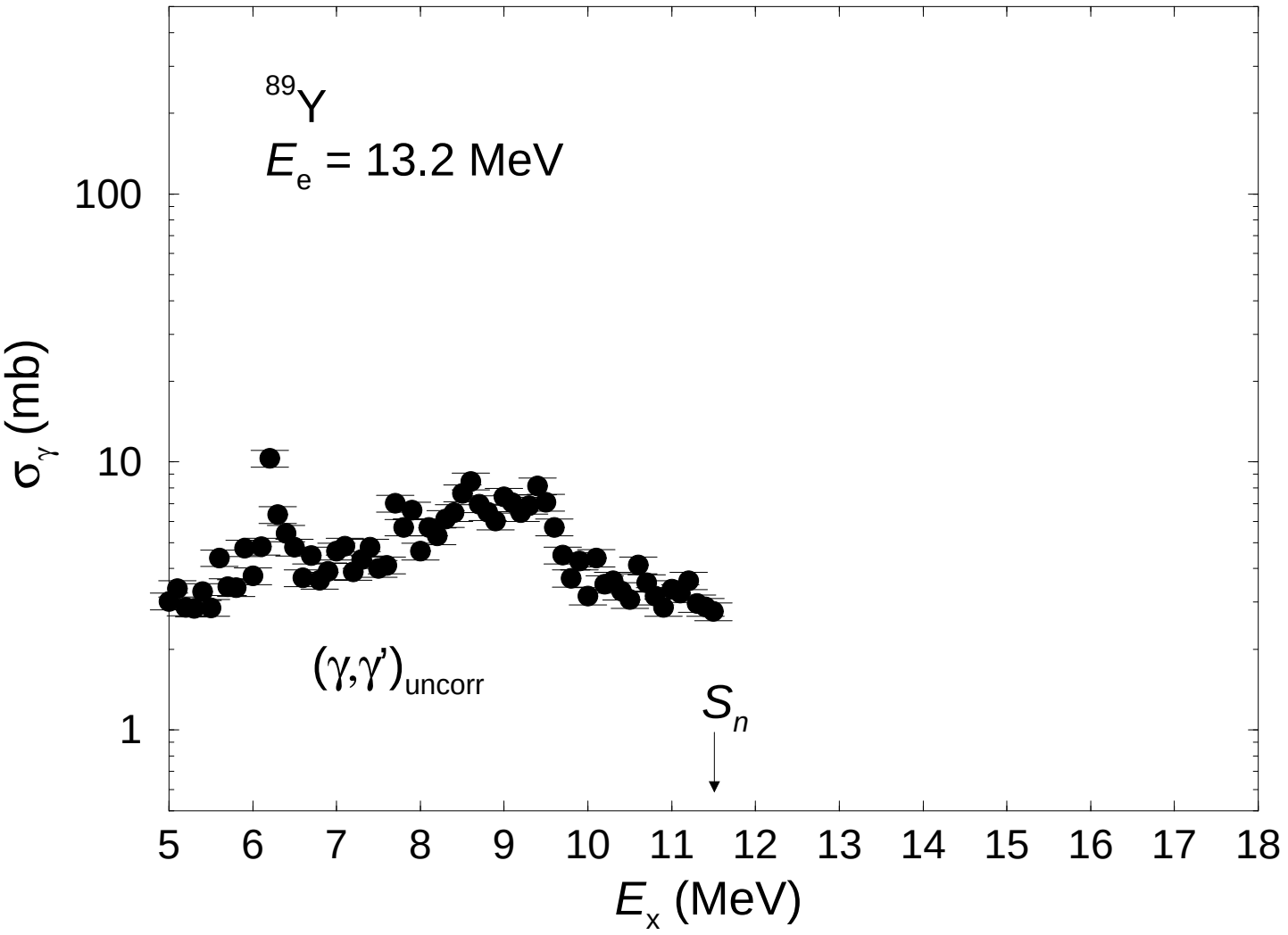

Present (γ, γ) data

Absorption cross section in ^{89}Y

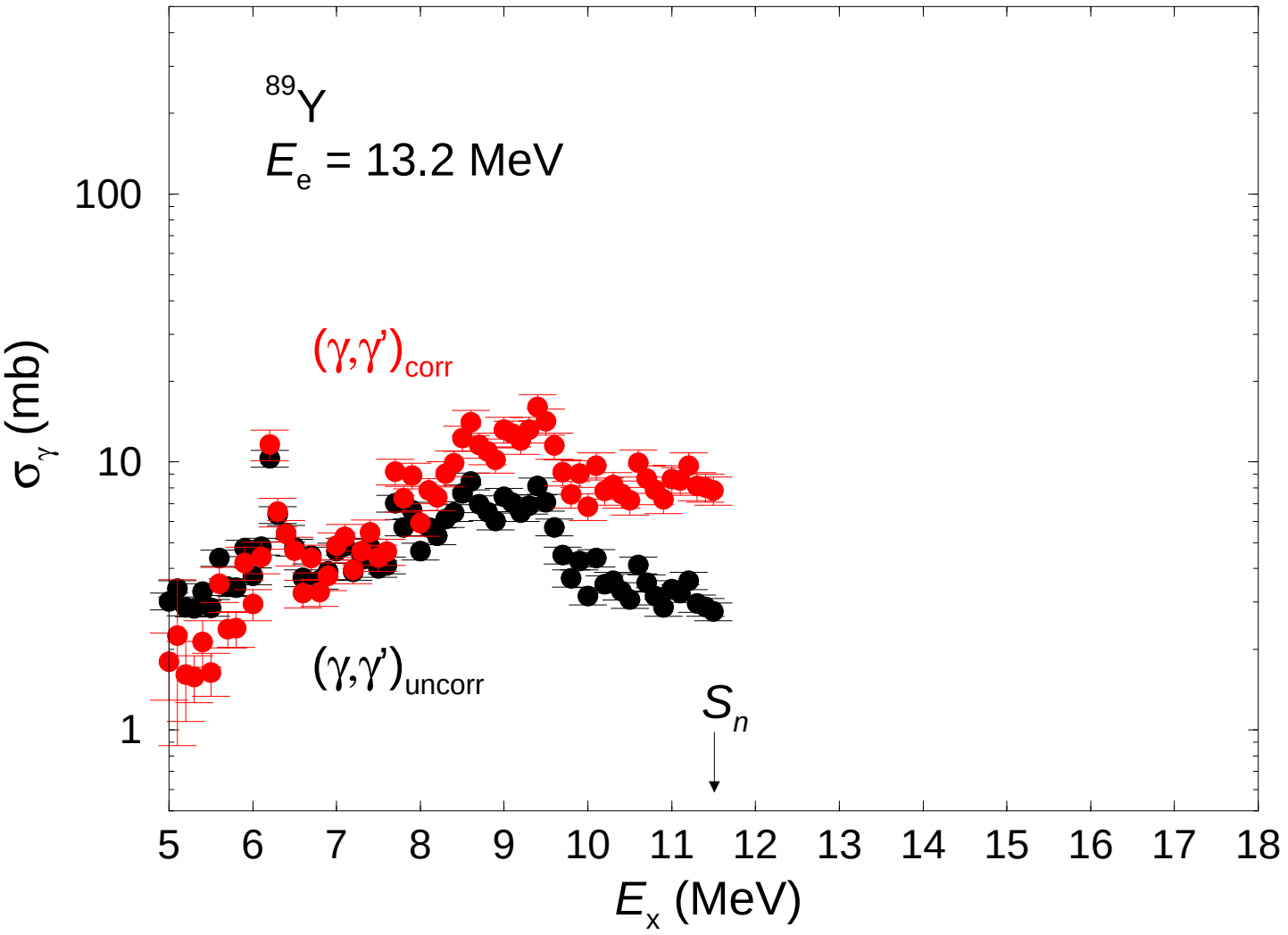

Present (γ, γ) data

Absorption cross section in ^{89}Y

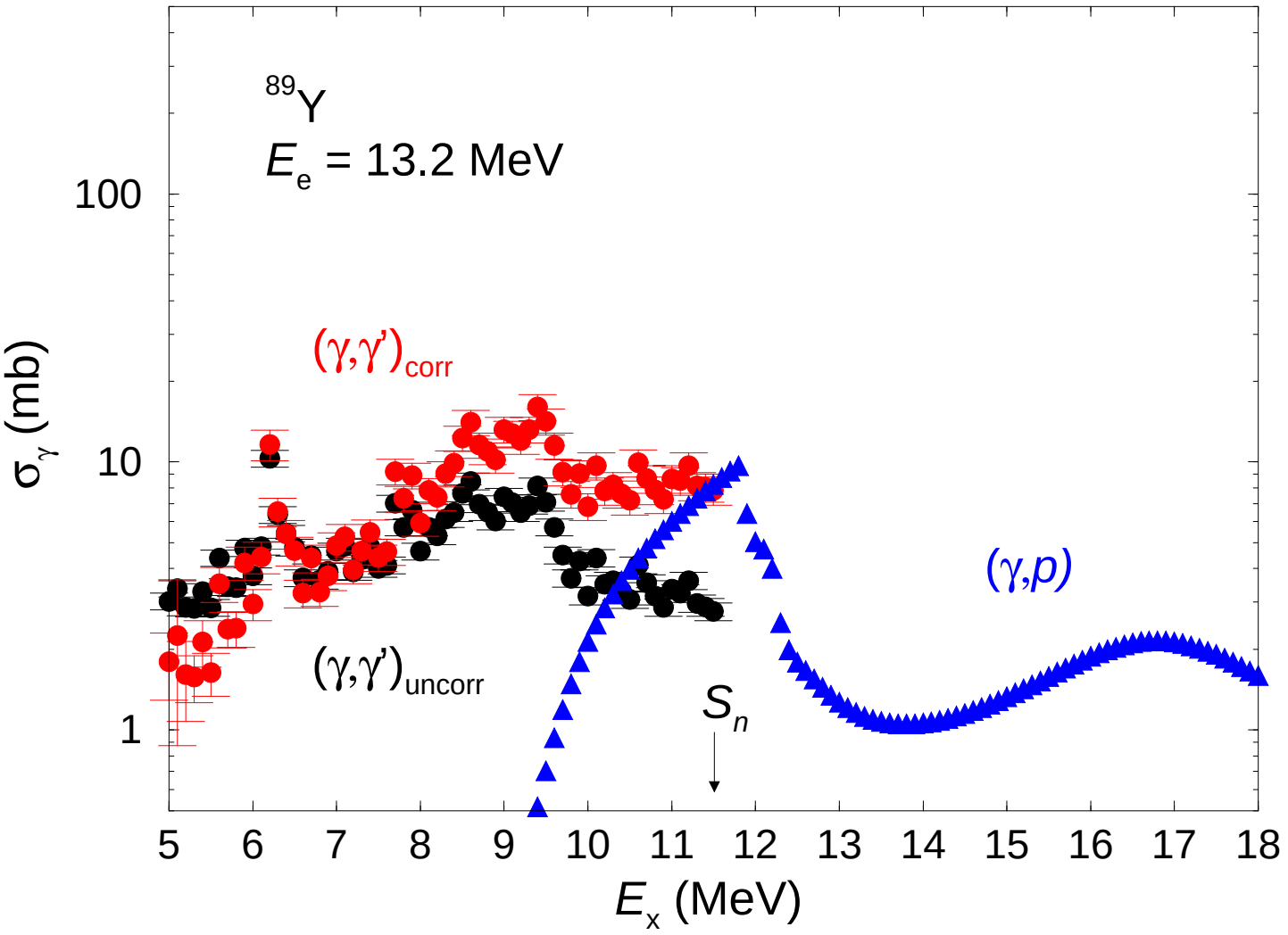

Present (γ, γ) data

(γ, p) calculated Talys

Absorption cross section in ^{89}Y

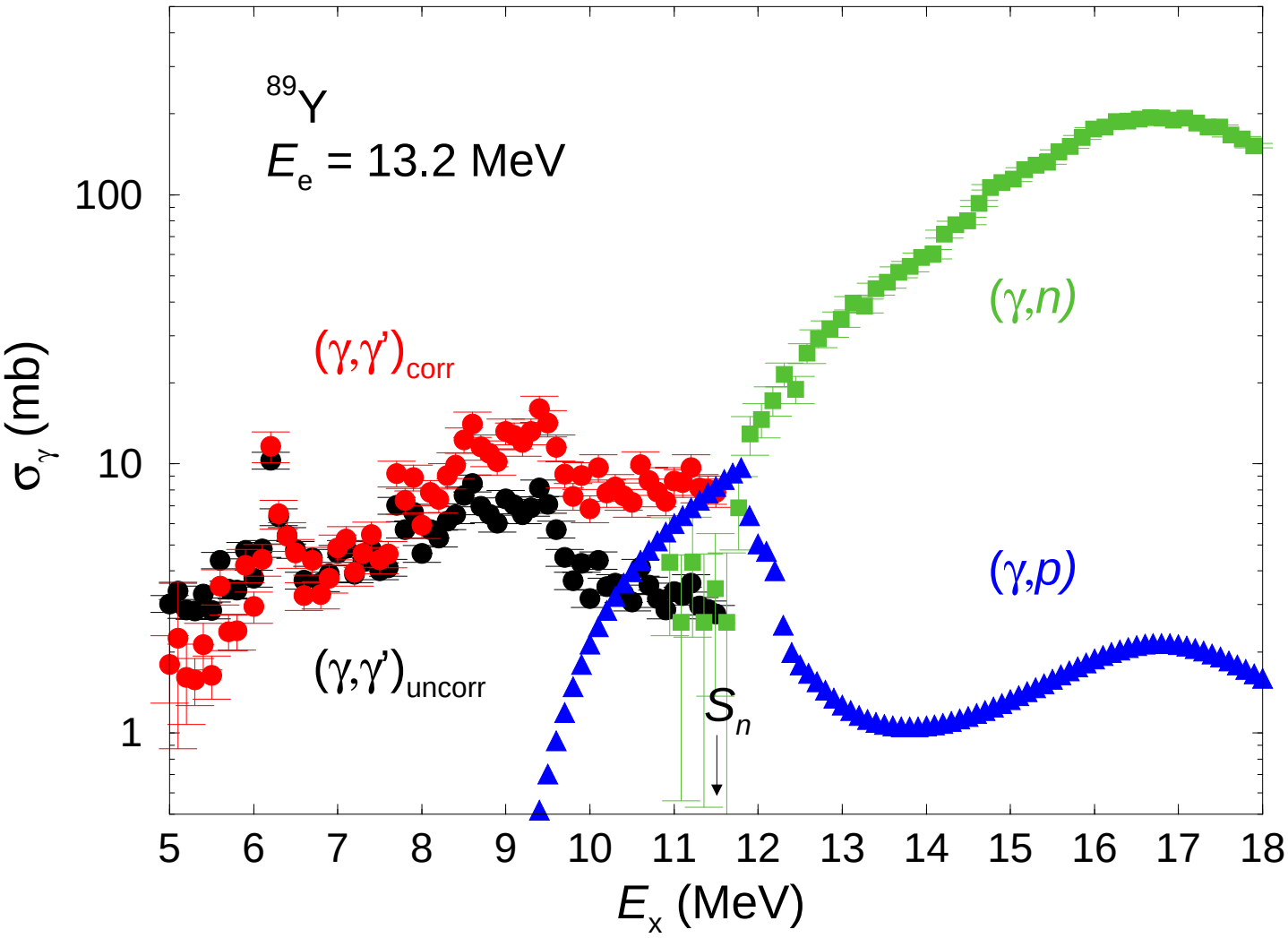

Present (γ, γ) data

(γ, p) calculated
Talys

(γ, n) data
NPA 175 (1971) 609

Test of various E1 strength functions

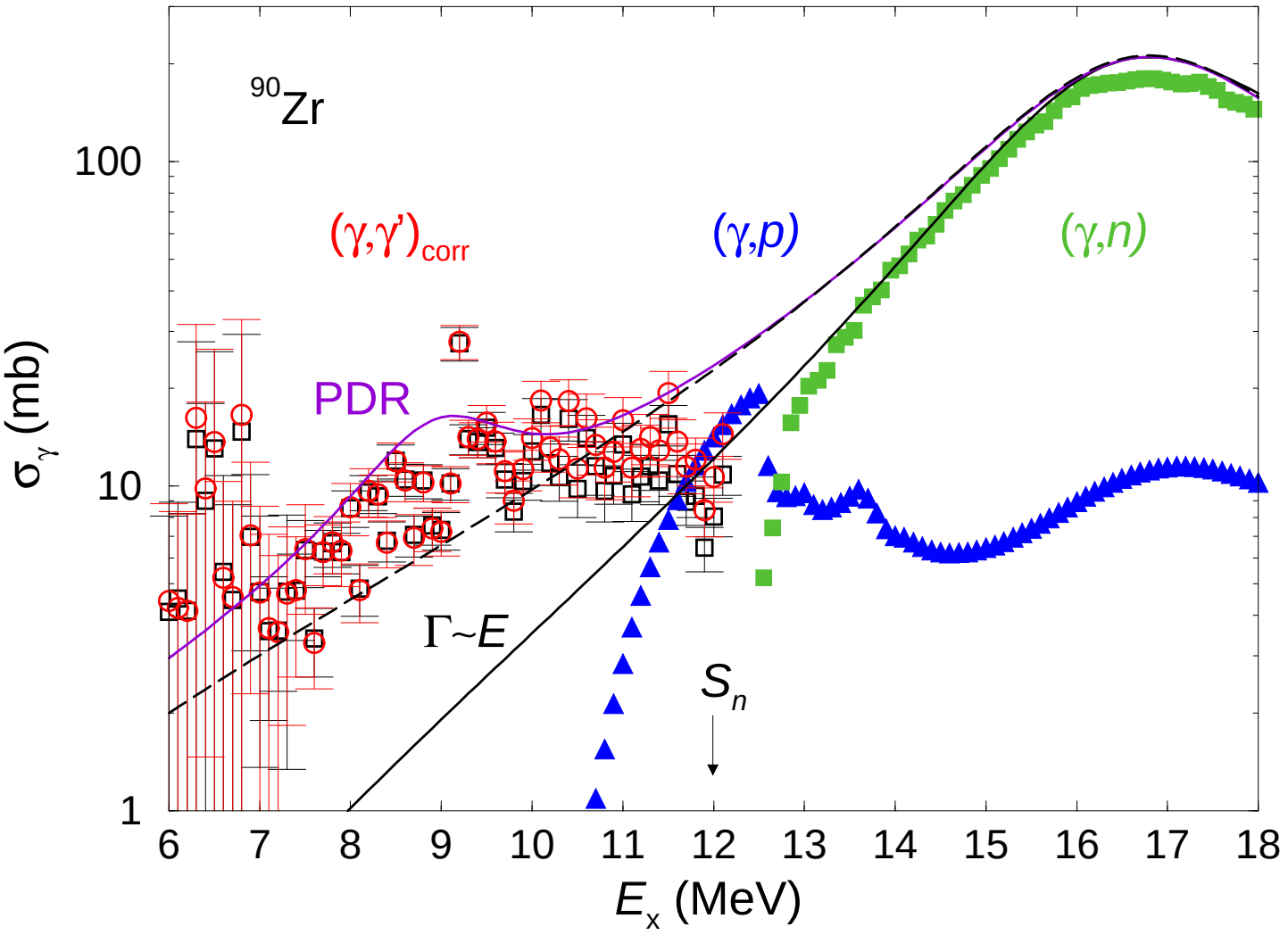

Lorentz curve + PDR

Lorentz curve with energy-dependent width

Test of level-density models

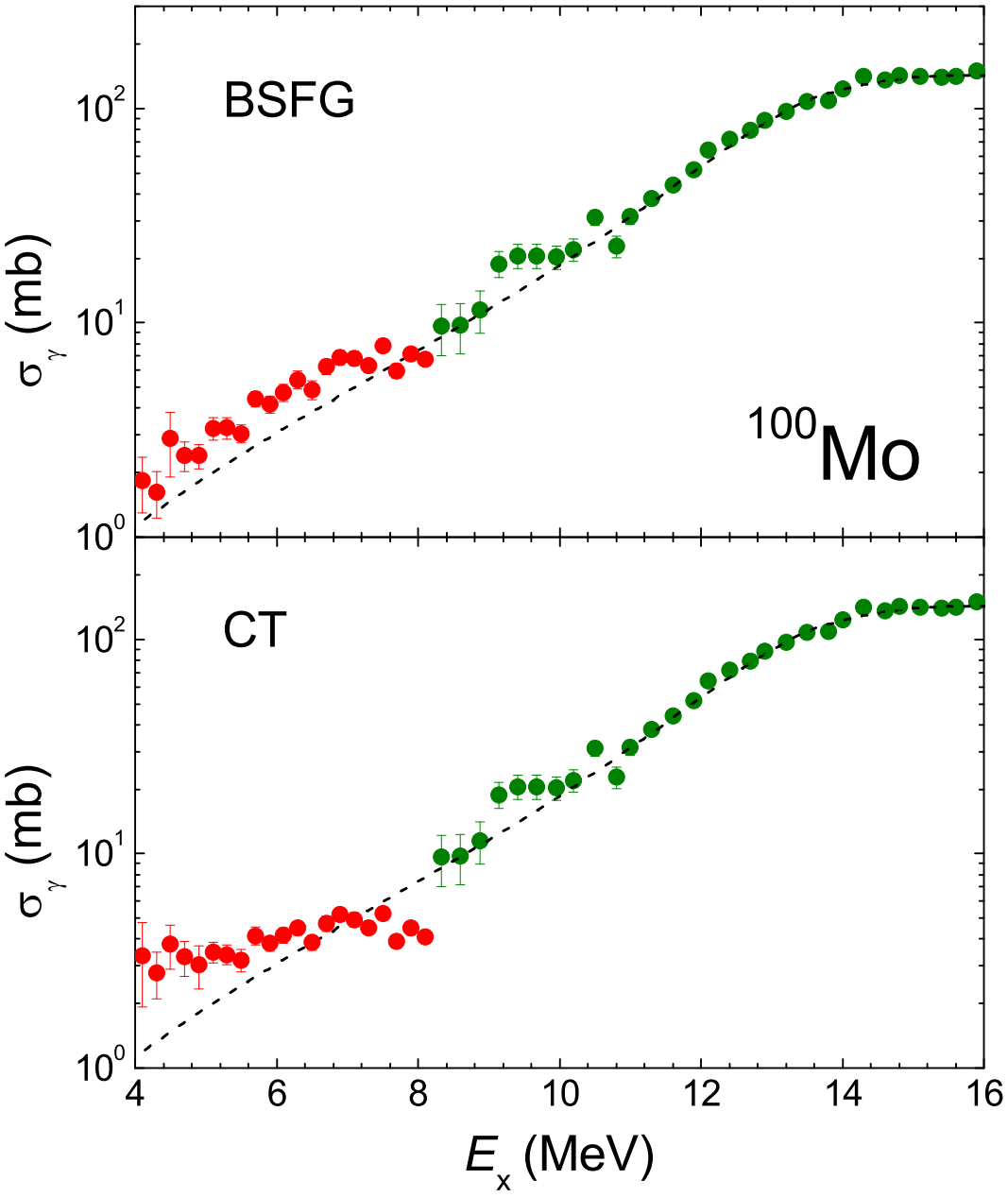

(γ,γ') data at $E_e^{kin} = 13.2$ MeV

(γ,n) data

Absorption cross section in ^{89}Y

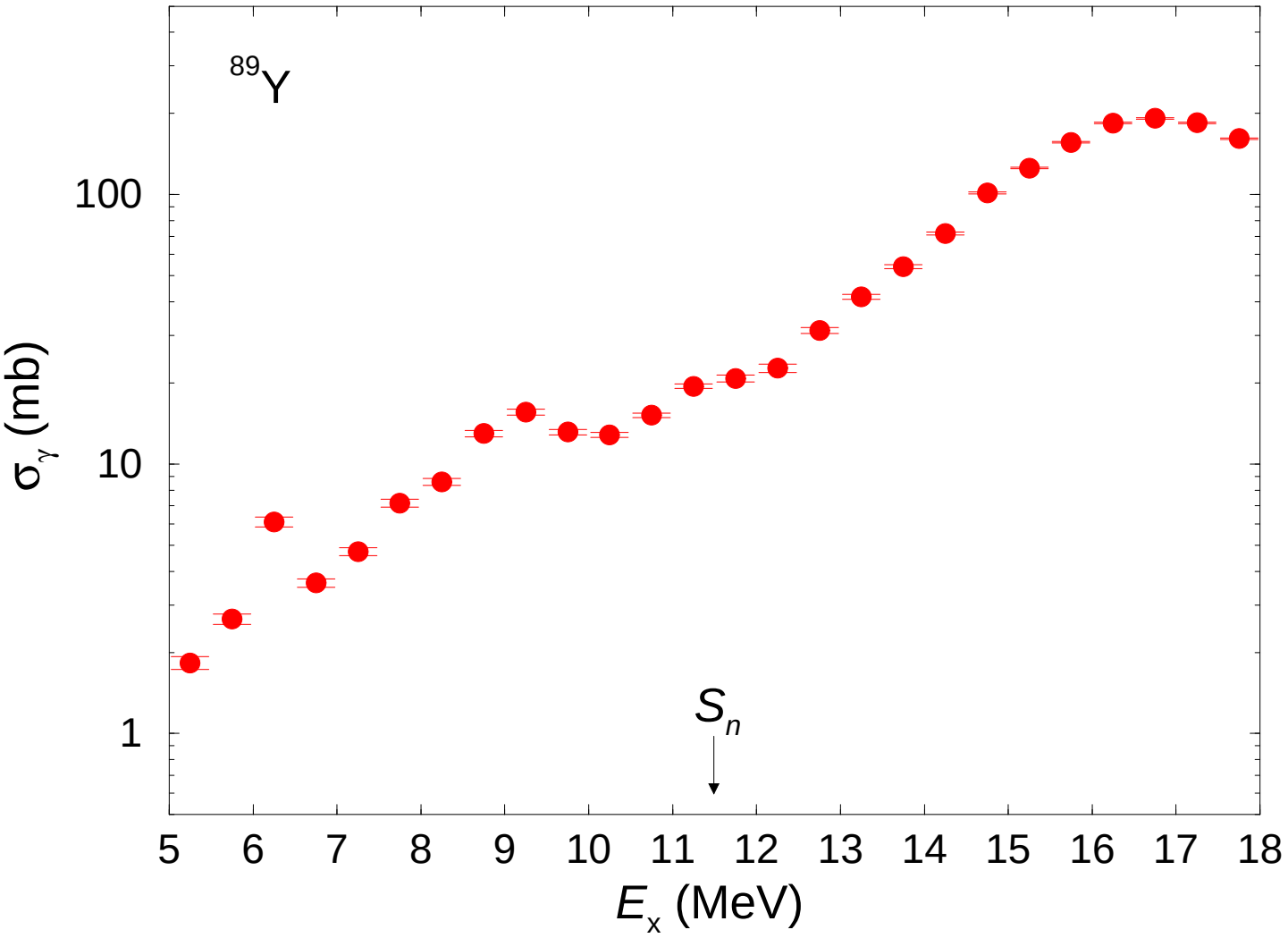

Present (γ, γ) data
$+ (\gamma, p)$ data
$+ (\gamma, n)$ data

Lorentz curve:

$E_0 = 16.8$ MeV

$\Gamma = 4.1$ MeV

$\frac{\pi}{2}\sigma_0\Gamma = 60\ \frac{NZ}{A}$ MeV mb

Absorption cross section in ^{89}Y

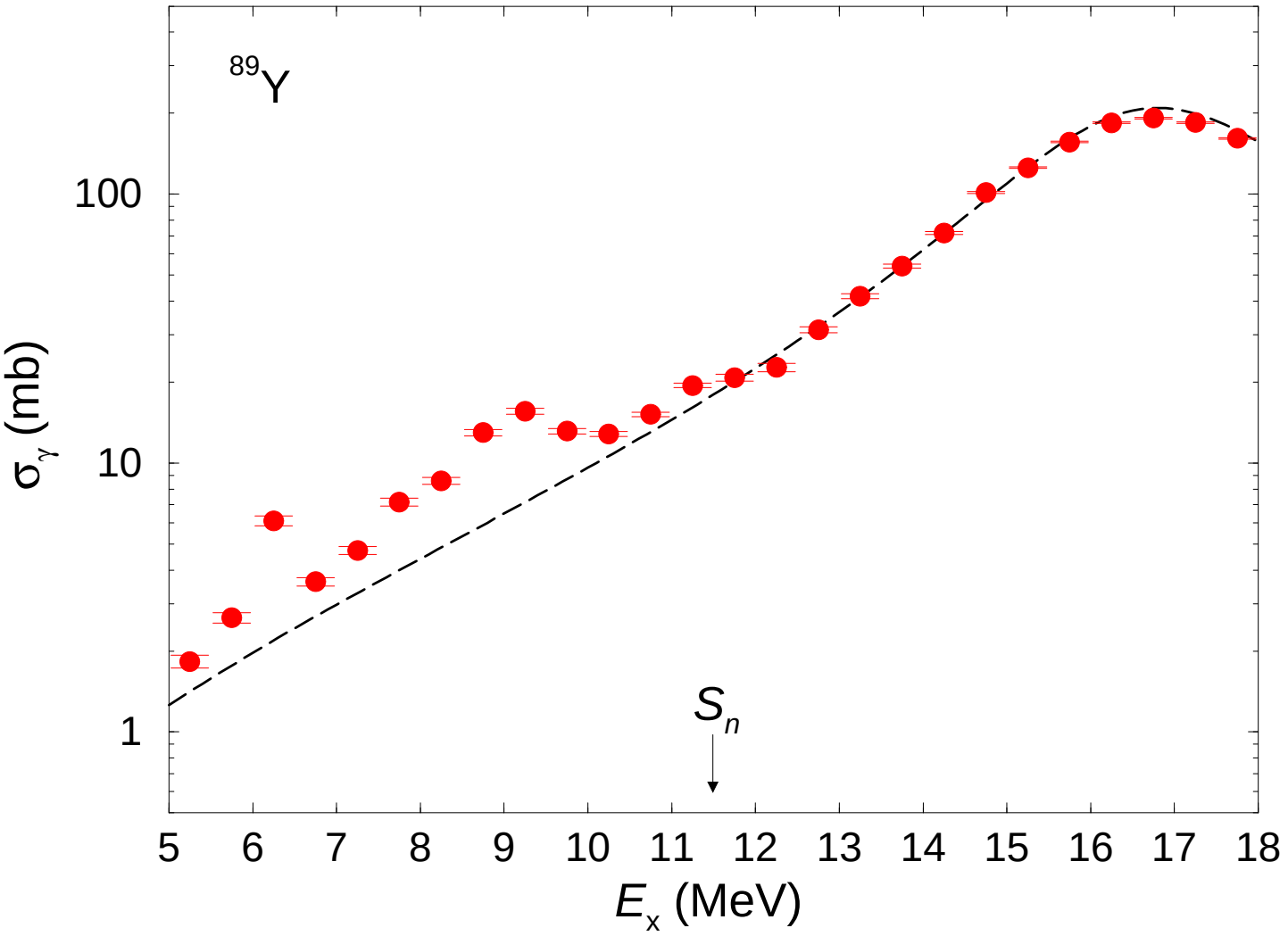

Present (γ, γ) data
$+ (\gamma, p)$ data
$+ (\gamma, n)$ data

Lorentz curve:
$E_0 = 16.8$ MeV
$\Gamma = 4.1$ MeV
$\frac{\pi}{2}\sigma_0\Gamma = 60\ \frac{NZ}{A}$ MeV mb

Absorption cross section in ^{89}Y

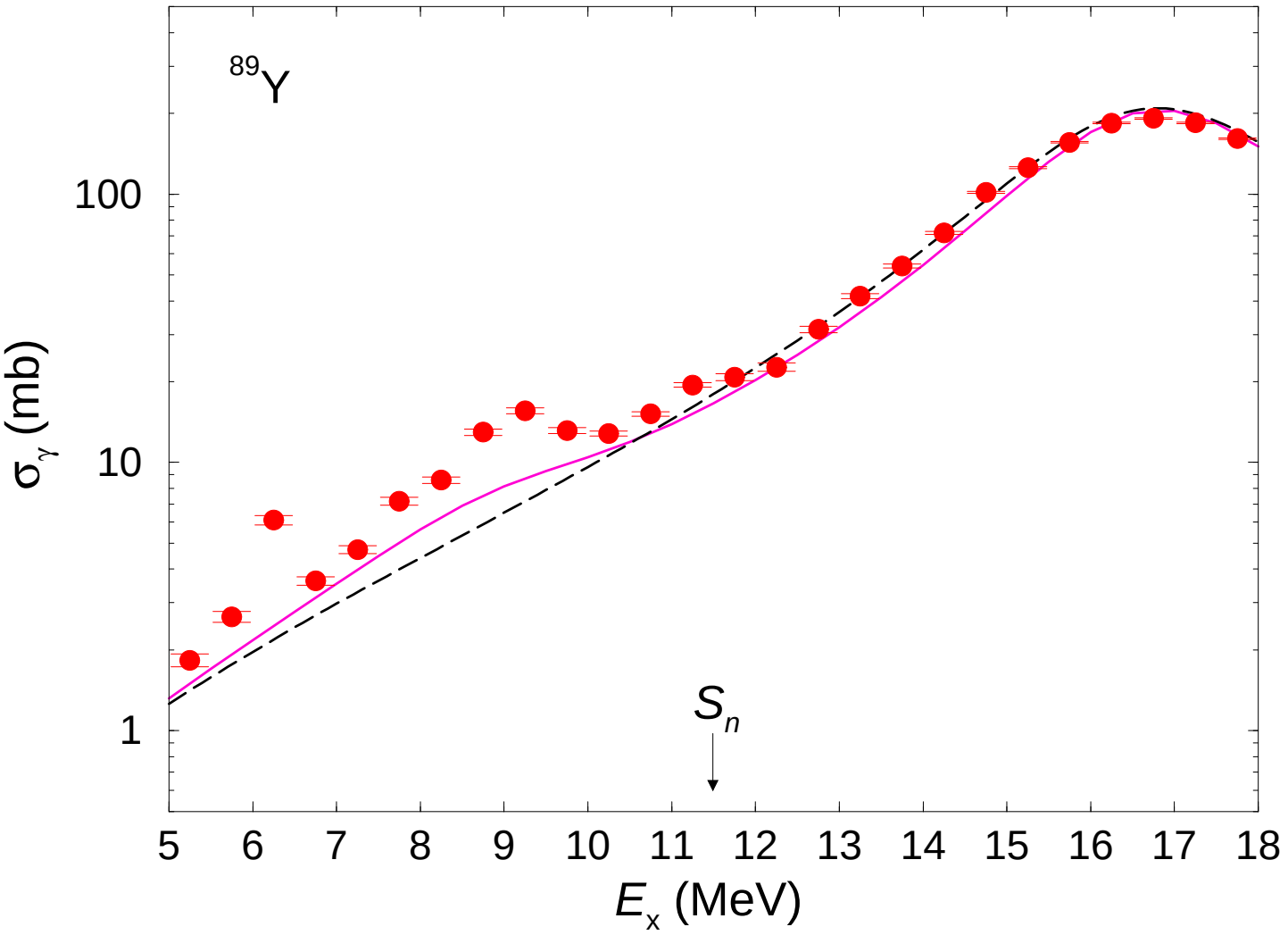

Present (γ, γ) data
$+ (\gamma, p)$ data
$+ (\gamma, n)$ data

Lorentz curve

Axel-Brink + M1

Absorption cross section in ^{89}Y

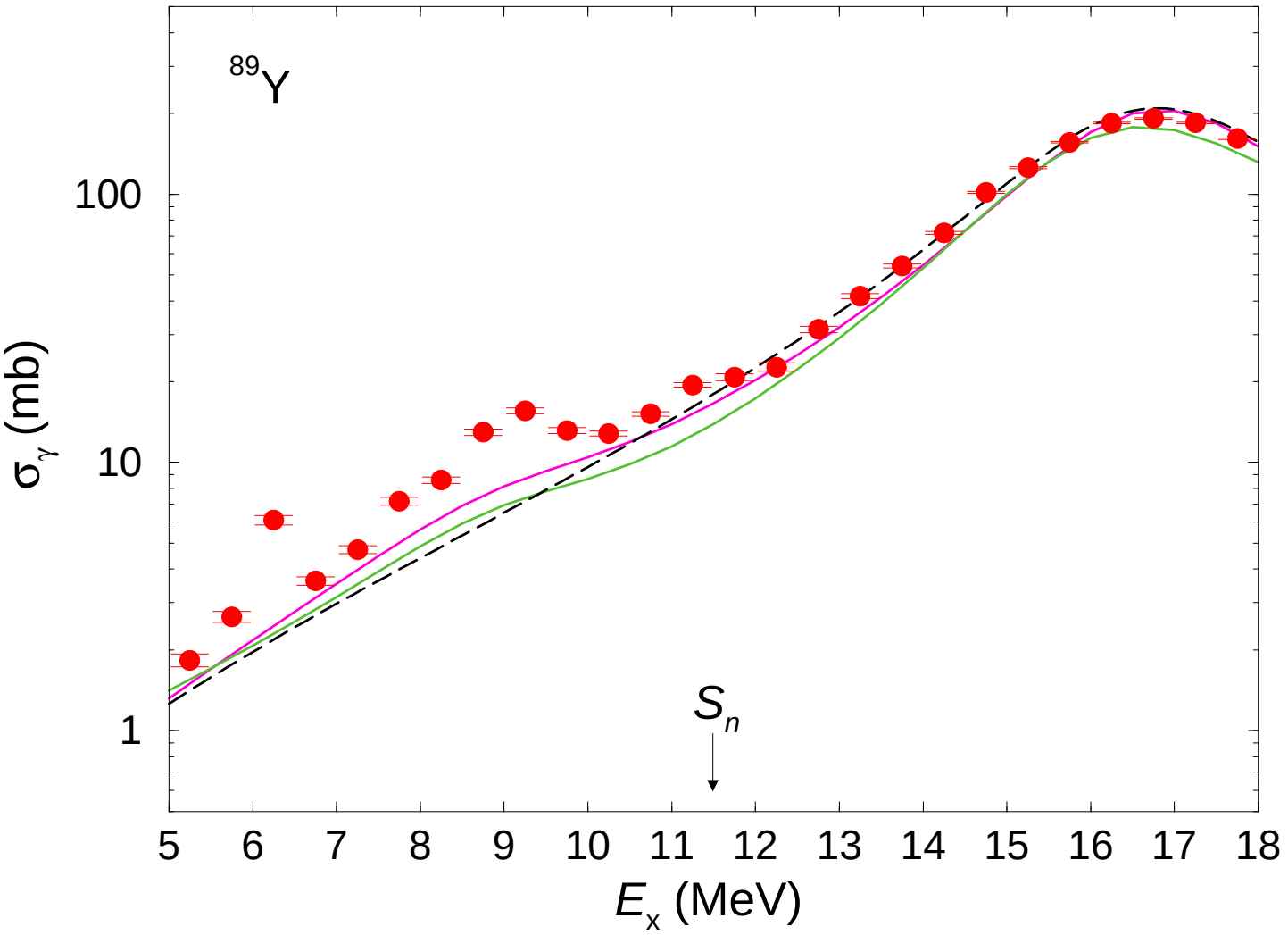

Present (γ, γ) data
$+ (\gamma, p)$ data
$+ (\gamma, n)$ data

Lorentz curve

Axel-Brink + M1

Kopecky-Uhl + M1

Absorption cross section in ^{89}Y

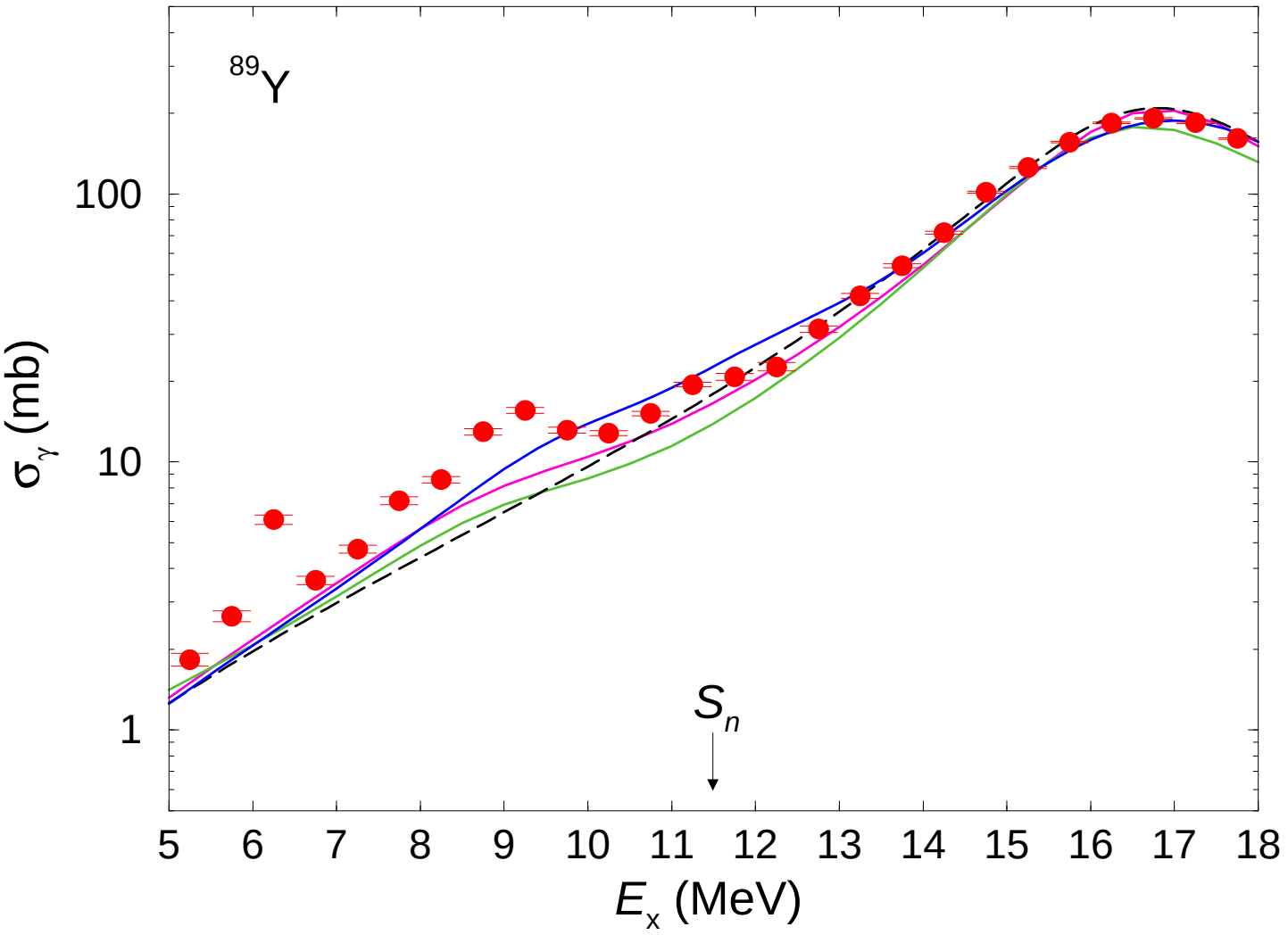

Present (γ, γ) data
$+ (\gamma, p)$ data
$+ (\gamma, n)$ data

Lorentz curve

Axel-Brink + M1

Kopecky-Uhl + M1

QRPA
Woods-Saxon basis
$\Gamma = 3.2$ MeV

Absorption cross sections in Mo isotopes

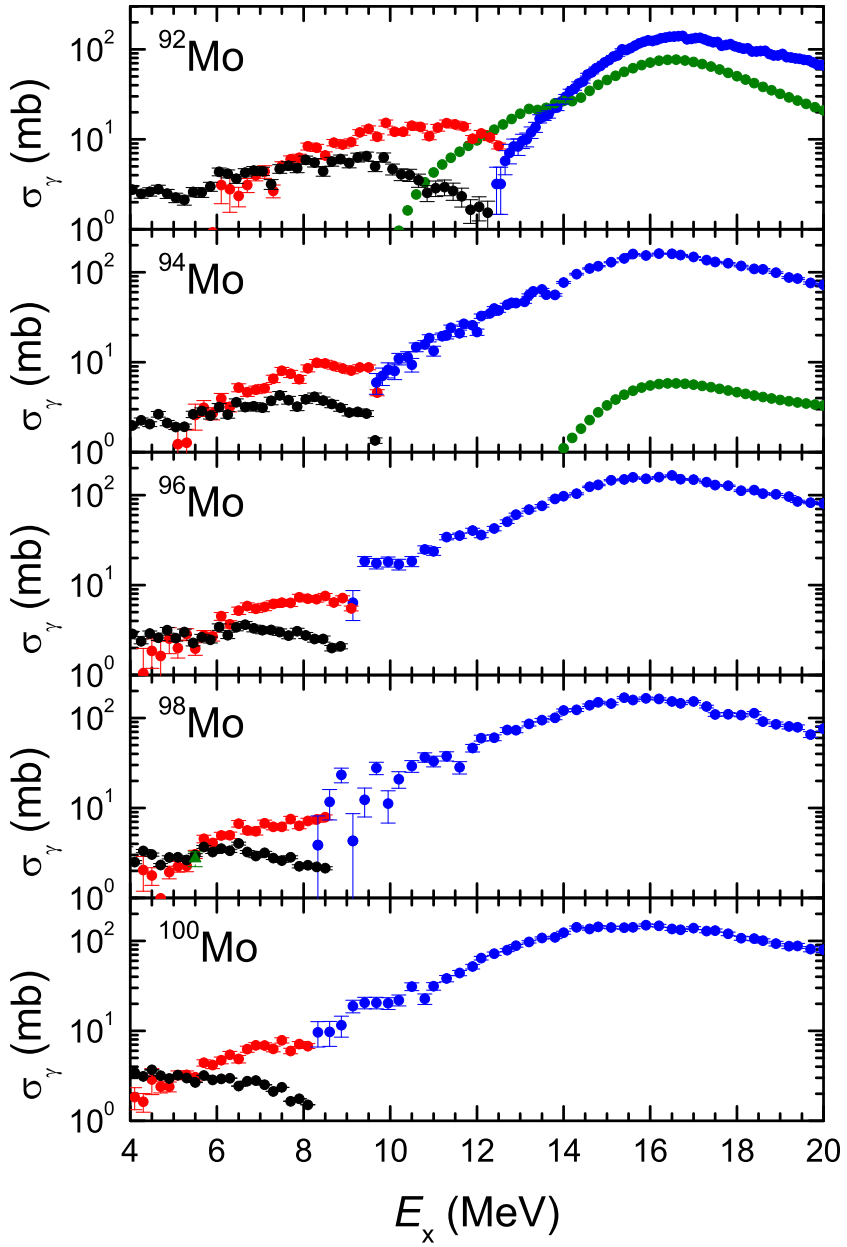

$$\sigma_\gamma(E_x) = \frac{2S_{\mathrm{TRK}}}{3\pi} \sum_{i=1}^{3} \frac{E_x^2 \Gamma_i(E_x)}{(E_i^2 - E_x^2)^2 + E_x^2 \Gamma_i^2(E_x)}$$

$$\Gamma_i(E_x) = \Gamma_S \cdot (E_x/E_i)^\delta; \quad \Gamma_S = 4 \text{ MeV}; \quad \delta \approx 0$$

$$S_{\mathrm{TRK}} = \int_0^\infty \sigma_\gamma(E)\, dE = 60 \frac{NZ}{A} \text{ MeV mb}$$

$$E_i = \hbar\omega_0 \left(1 - \frac{2}{3}\,\epsilon_2 \cos\left(\gamma - \frac{2\pi i}{3}\right)\right)$$

Absorption cross sections in Mo isotopes

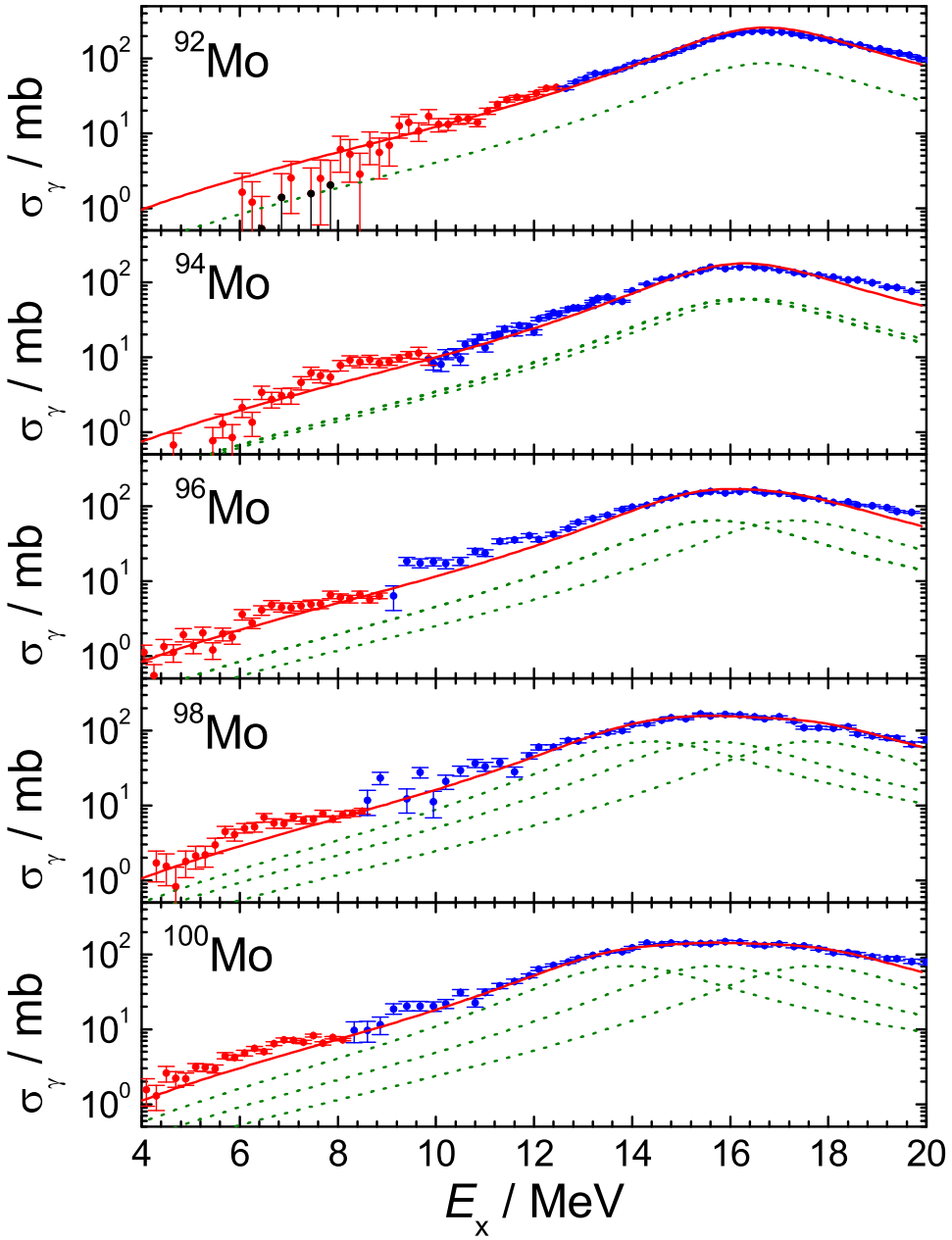

$$\sigma_\gamma(E_x) = \frac{2S_{\mathrm{TRK}}}{3\pi} \sum_{i=1}^{3} \frac{E_x^2 \Gamma_i(E_x)}{(E_i^2 - E_x^2)^2 + E_x^2 \Gamma_i^2(E_x)}$$

$$\Gamma_i(E_x) = \Gamma_S \cdot (E_x/E_i)^\delta; \quad \Gamma_S = 4 \text{ MeV}; \quad \delta \approx 0$$

$$S_{\mathrm{TRK}} = \int_0^\infty \sigma_\gamma(E)\, dE = 60 \frac{NZ}{A} \text{ MeV mb}$$

$$E_i = \hbar\omega_0 \left(1 - \frac{2}{3}\,\epsilon_2 \cos\left(\gamma - \frac{2\pi i}{3}\right)\right)$$

Absorption cross sections in Mo isotopes

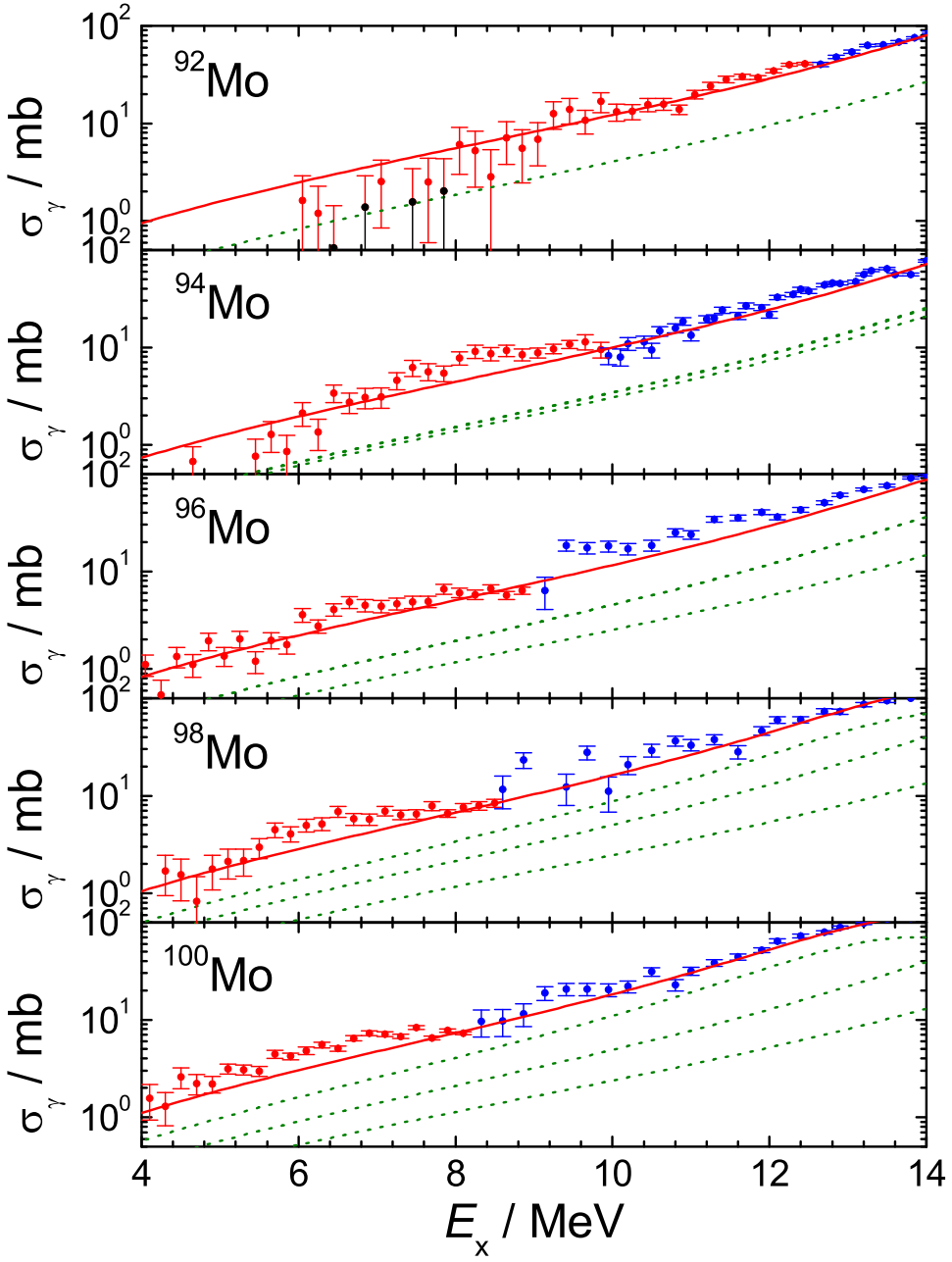

$$\sigma_\gamma(E_x) = \frac{2S_{\mathrm{TRK}}}{3\pi} \sum_{i=1}^{3} \frac{E_x^2 \Gamma_i(E_x)}{(E_i^2 - E_x^2)^2 + E_x^2 \Gamma_i^2(E_x)}$$

$$\Gamma_i(E_x) = \Gamma_S \cdot (E_x/E_i)^\delta; \quad \Gamma_S = 4 \text{ MeV}; \quad \delta \approx 0$$

$$S_{\mathrm{TRK}} = \int_0^\infty \sigma_\gamma(E)\, dE = 60 \frac{NZ}{A} \text{ MeV mb}$$

$$E_i = \hbar\omega_0 \left(1 - \frac{2}{3}\,\epsilon_2 \cos\left(\gamma - \frac{2\pi i}{3}\right)\right)$$

QRPA calculations in a deformed basis for Mo isotopes

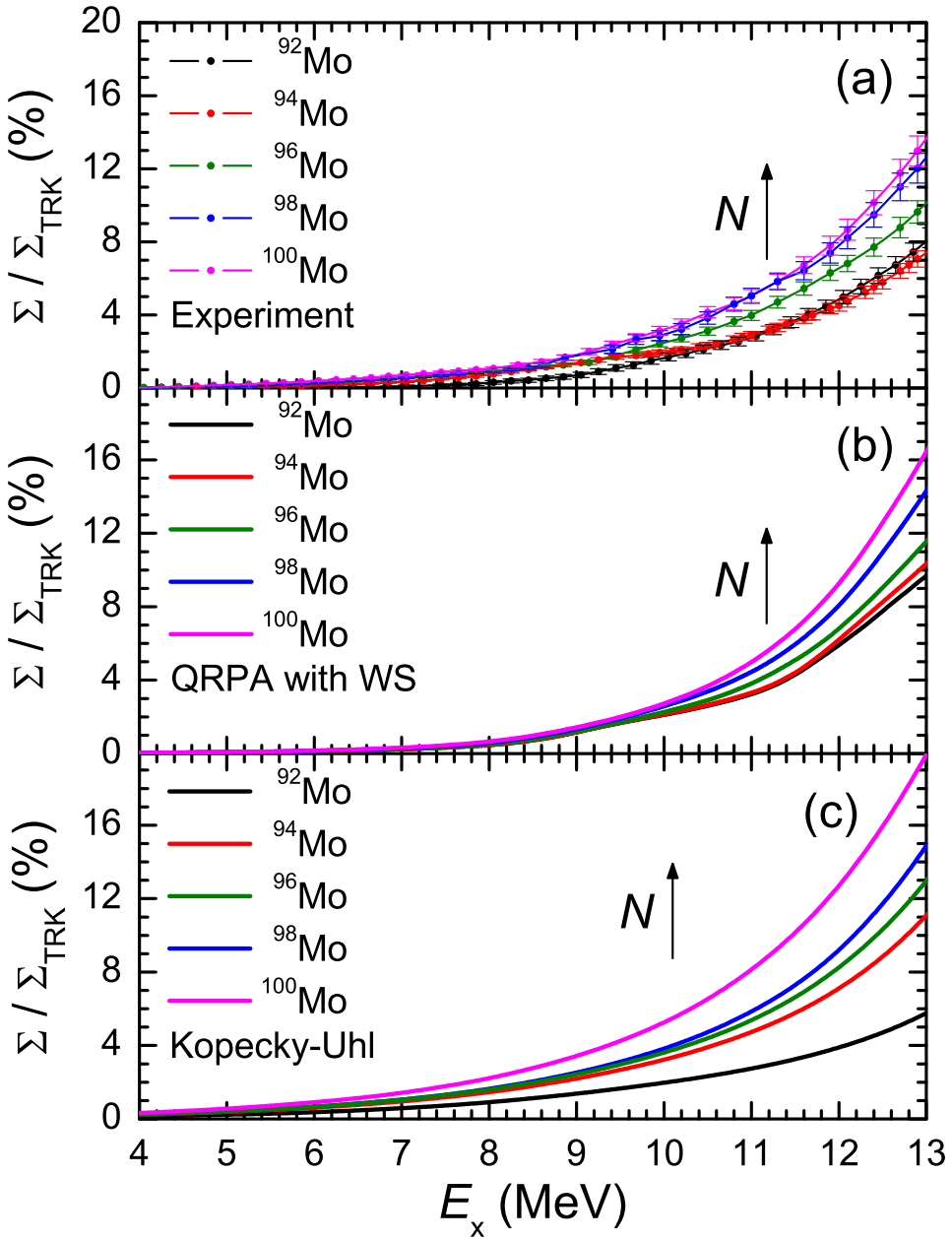

$$\Sigma(E_x) = \sum_{i}^{E_x} \sigma_\gamma(E_i)\ \Delta E$$

$$\Sigma_{TRK} = \int_0^\infty \sigma_\gamma(E)\ dE = 60\frac{NZ}{A}\ \text{MeV mb}$$

QRPA calculations for deformed nuclei

Hamiltonian for 1^- states:

- Nilsson or Woods-Saxon mean field plus monopole pairing
- isoscalar and isovector dipole-dipole and octupole-octupole interactions

F. Dönau, PRL 94 (2005) 092503, F. Dönau et al., PRC 76 (2007) 014317

Total energy as a function of the quadrupole deformation ε_2 and the triaxiality γ:

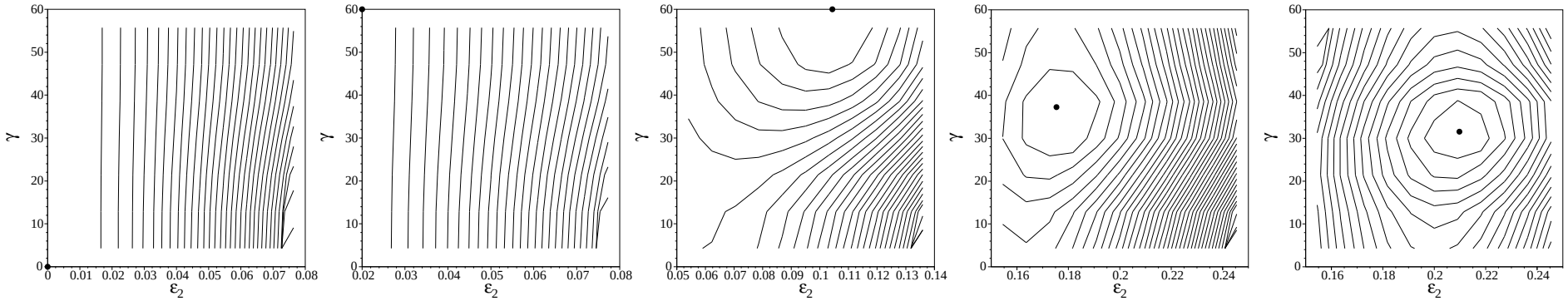

$^{92}Mo_{50}$	$^{94}Mo_{52}$	$^{96}Mo_{54}$	$^{98}Mo_{56}$	$^{100}Mo_{58}$
$\varepsilon_2 = 0.0$	$\varepsilon_2 = 0.02$	$\varepsilon_2 = 0.10$ $\gamma = 60^\circ$	$\varepsilon_2 = 0.18$ $\gamma = 37^\circ$	$\varepsilon_2 = 0.21$ $\gamma = 32^\circ$

TAC model with shell-correction method:

S. Frauendorf, NPA 557 (1993) 259c, NPA 667 (2000) 115

QRPA calculations in a deformed basis for Mo isotopes

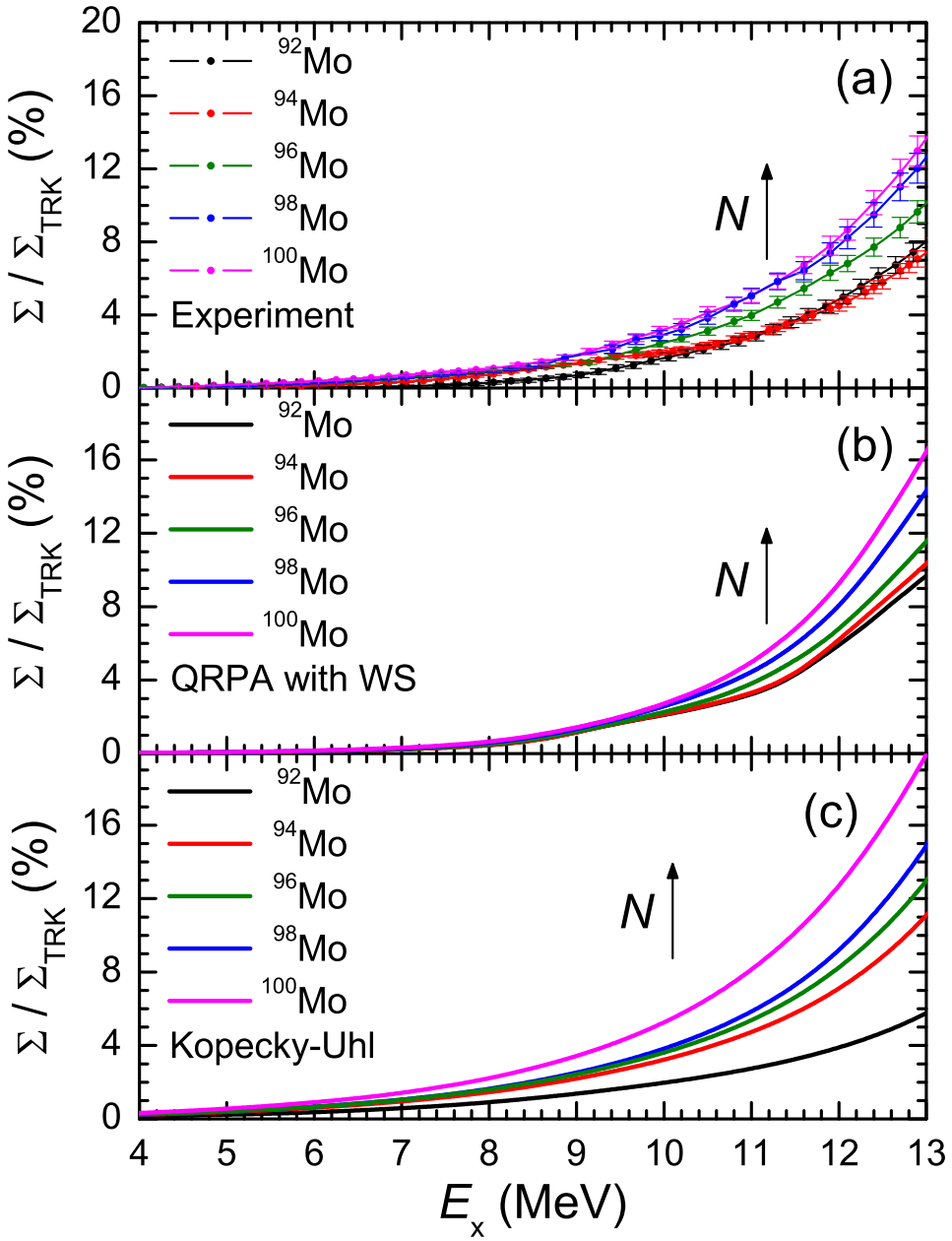

$$\Sigma(E_x) = \sum_{i}^{E_x} \sigma_\gamma(E_i)\ \Delta E$$

$$\Sigma_{TRK} = \int_0^\infty \sigma_\gamma(E)\ dE = 60\frac{NZ}{A}\ \text{MeV mb}$$

Absorption cross sections in Mo isotopes

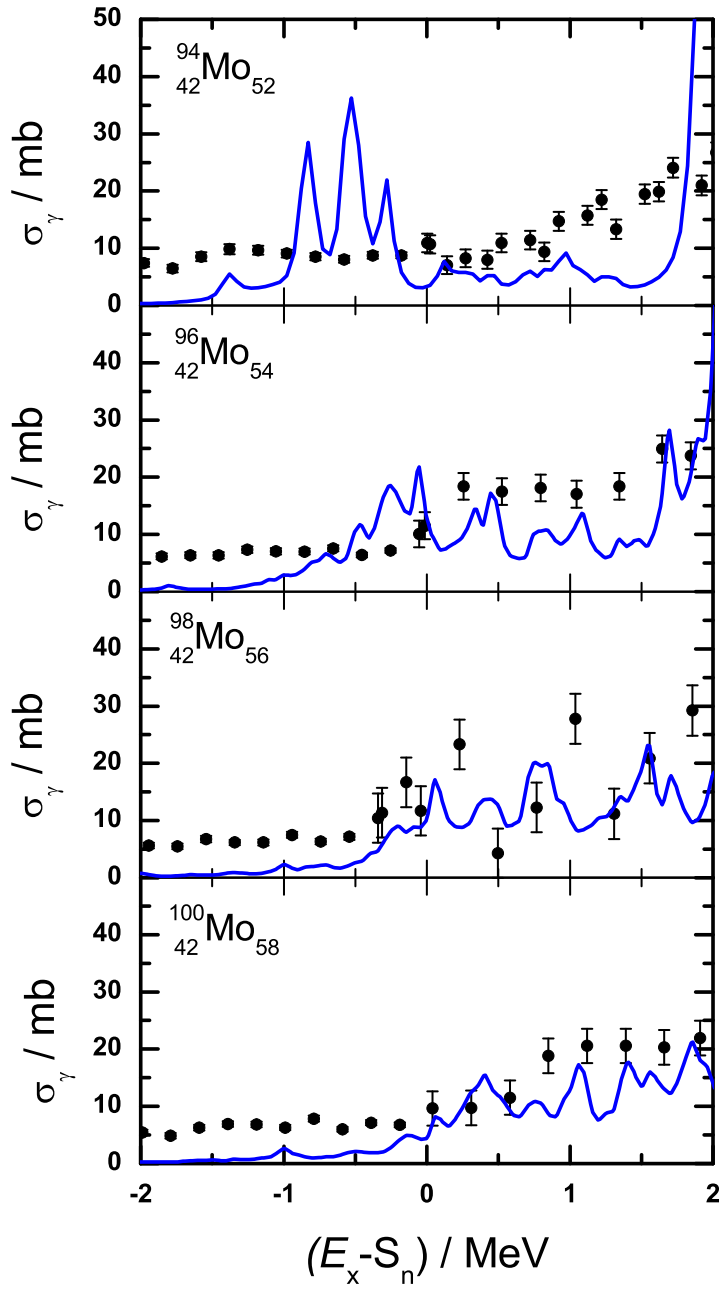

Present (γ, γ) data + (γ, p) data + (γ, n) data

QRPA, folded with Lorentzian, $\Gamma = 0.1$ MeV

Absorption cross section in ^{90}Zr

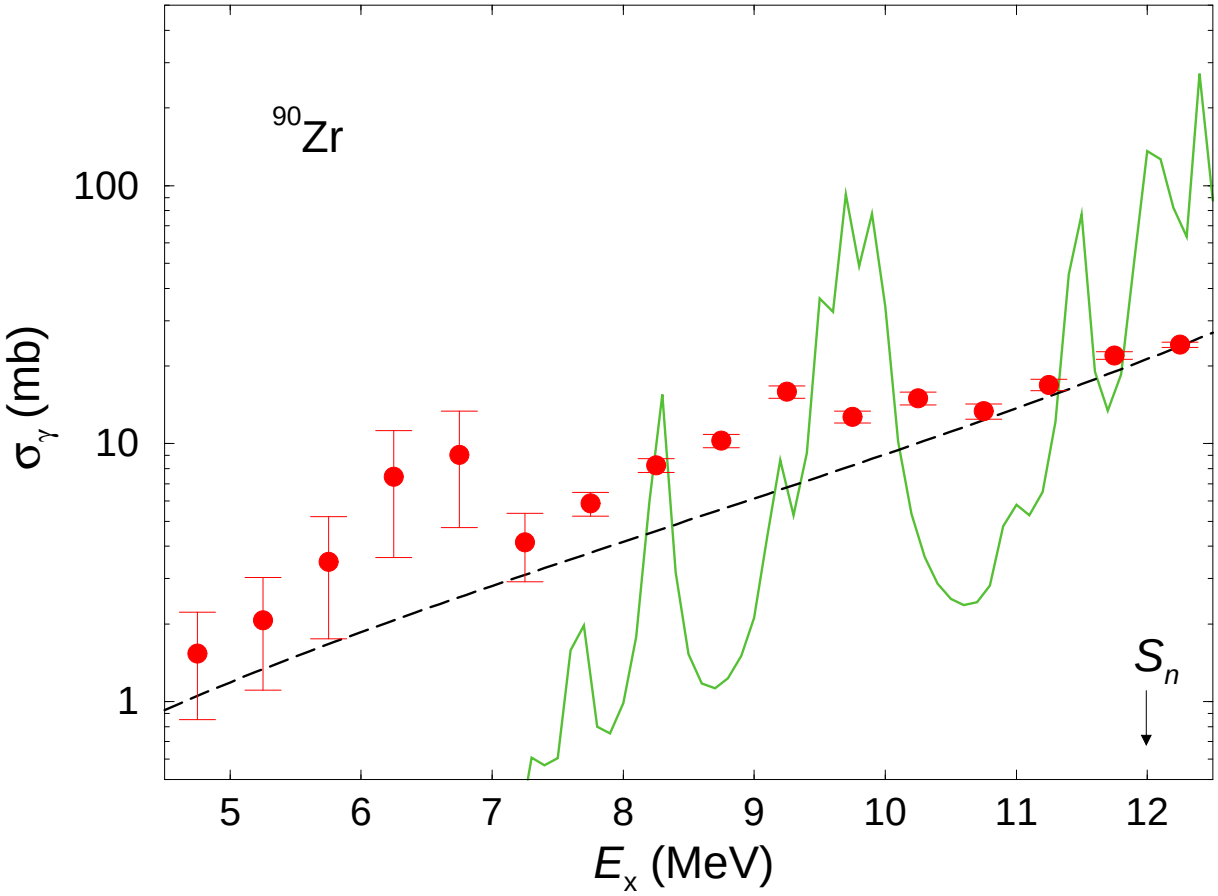

Present (γ, γ) data
+ (γ, p) data
+ (γ, n) data

Lorentz curve:
$E_0 = 16.8$ MeV
$\Gamma = 4.0$ MeV
$\frac{\pi}{2}\sigma_0\Gamma = 60\ \frac{NZ}{A}$ MeV mb

QRPA, folded with
Lorentzian, $\Gamma = 0.1$ MeV

Absorption cross section in ^{90}Zr

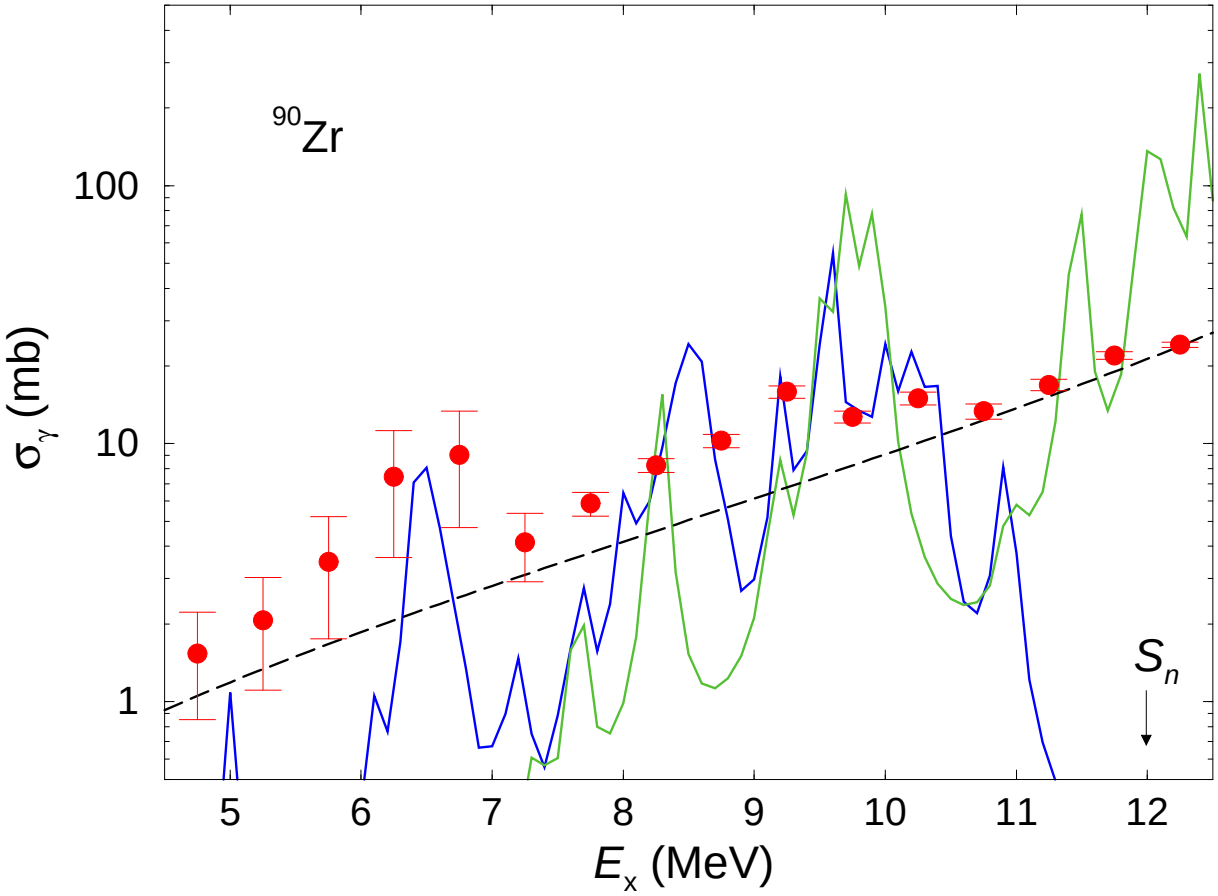

Present (γ, γ) data
$+ (\gamma, p)$ data
$+ (\gamma, n)$ data

Lorentz curve:
$E_0 = 16.8$ MeV
$\Gamma = 4.0$ MeV
$\frac{\pi}{2}\sigma_0\Gamma = 60\ \frac{NZ}{A}$ MeV mb

QRPA, folded with
Lorentzian, $\Gamma = 0.1$ MeV

QPM, folded with
Lorentzian, $\Gamma = 0.1$ MeV

By courtesy of N. Tsoneva

Absorption cross sections in Mo isotopes

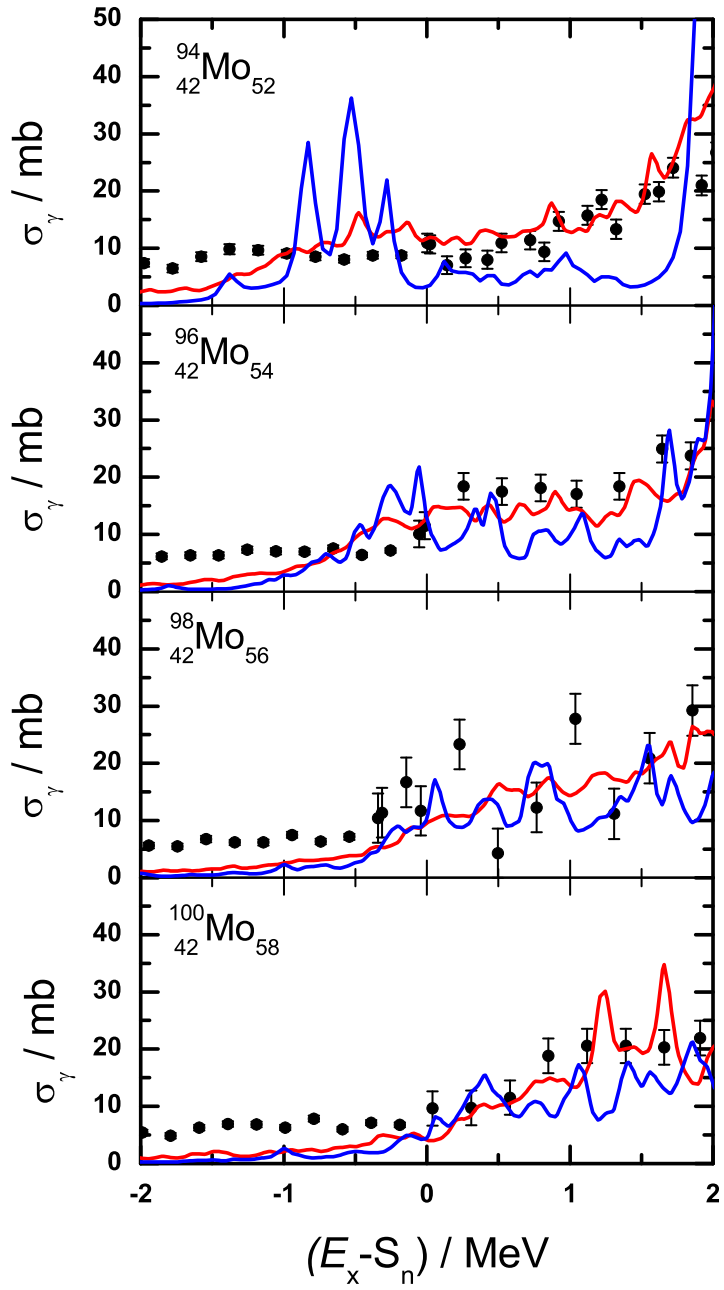

Present (γ, γ) data + (γ, p) data + (γ, n) data

QRPA, folded with Lorentzian, $\Gamma = 0.1$ MeV

ISS-QRPA, folded with Lorentzian, $\Gamma = 0.1$ MeV

Absorption cross sections in Mo isotopes

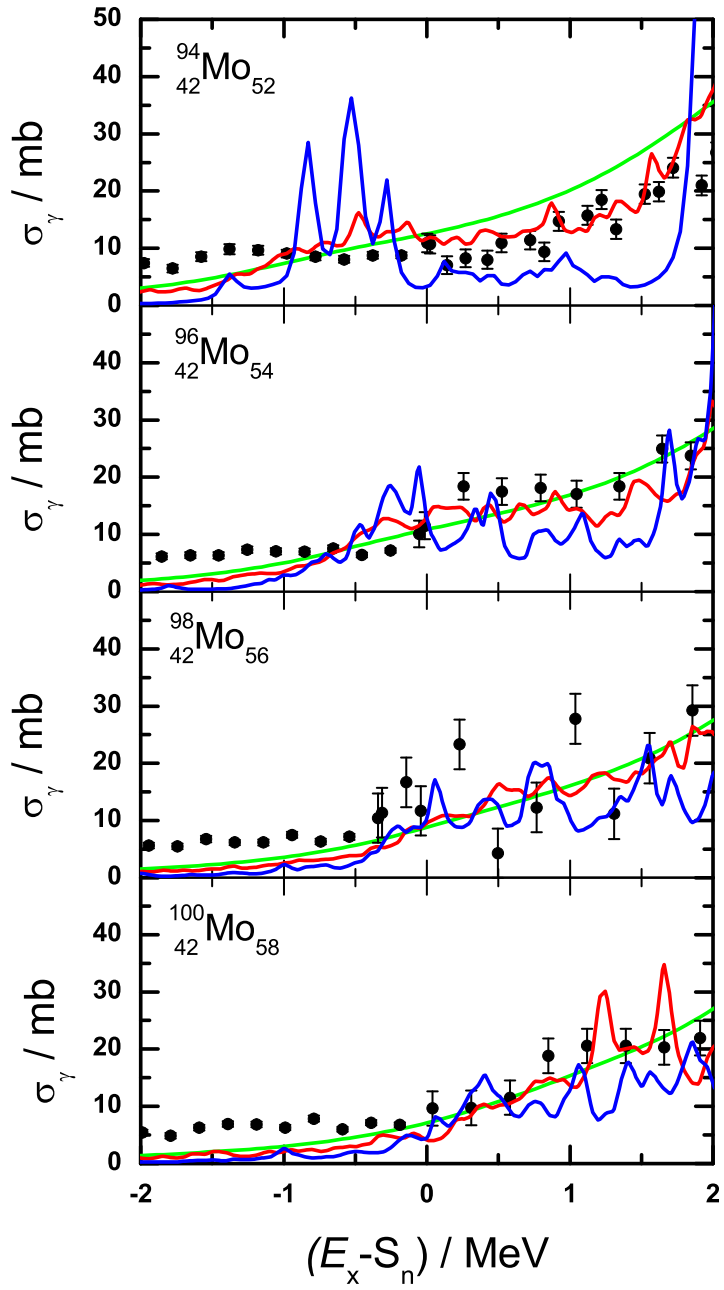

Present (γ, γ) data + (γ, p) data + (γ, n) data

QRPA, folded with Lorentzian, $\Gamma = 0.1$ MeV

ISS-QRPA, folded with Lorentzian, $\Gamma = 0.1$ MeV

ISS-QRPA, folded with Lorentzian, $\Gamma = 0.014/\text{MeV}\ E^2$

Summary

- Study of dipole-strength distributions at high excitation energy and high level density via photon scattering.
- Simulations of statistical γ cascades: Estimate of intensities of inelastic transitions and correction of intensities of elastic transitions:
  - Correct determination of σ_γ up to the neutron-separation energy S_n including unresolved strength.
  - Combination with (γ,p) and (γ,n) data gives information on σ_γ over the whole energy range from low excitation energy up to the giant dipole resonance.
  - Observation of extra strength in the range from 6 to 12 MeV – not described in phenomenological approximations of dipole-strength functions.
- QRPA calculations describe the increase of dipole strength below S_n toward the heavier Mo isotopes as a consequence of increasing deformation.
- Instantaneous-shape sampling improves the description of the dipole strength around S_n in transitional nuclei.
- Further developments are necessary to reproduce the extra strength below S_n.

Absolute detector efficiency and photon flux

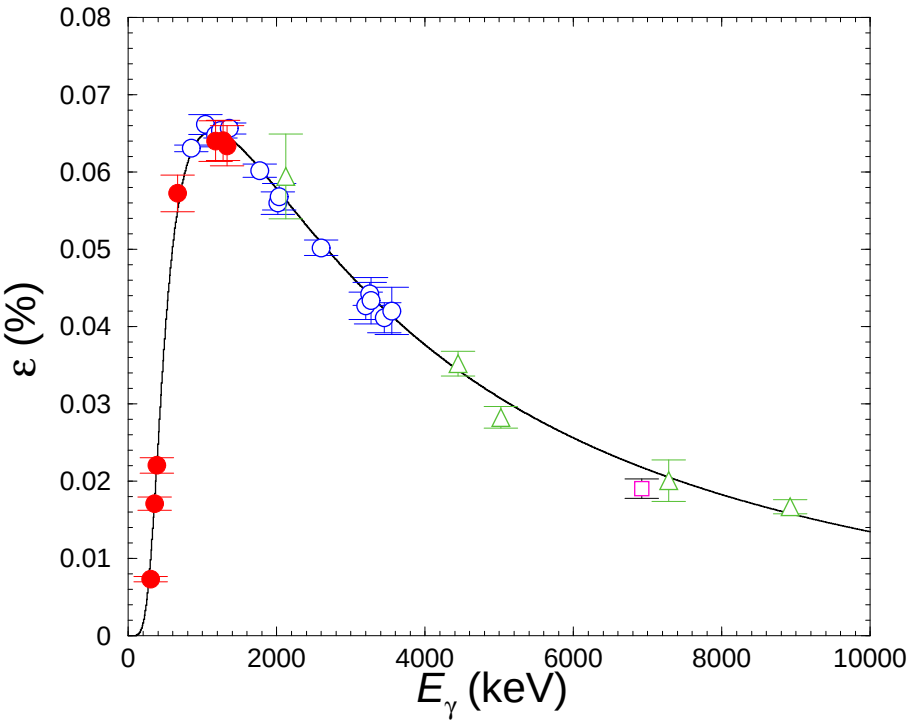

Absolute efficiency of two detectors at 127° deduced from ^{22}Na, ^{60}Co, ^{133}Ba, (filled circles) and simulated with GEANT3 (solid line). Relative efficiencies deduced from ^{56}Co (open circles), ^{11}B (open triangles) and ^{16}O (open square).

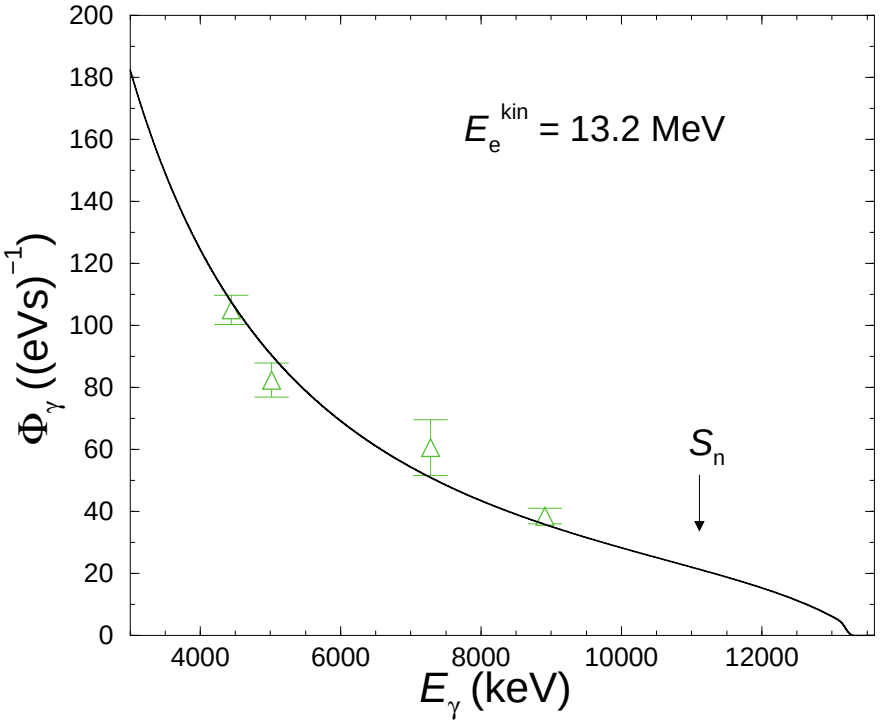

Absolute photon flux deduced from transitions in ^{11}B (open triangles) using the calculated efficiency shown in the left panel and relative photon flux calculated according to G. Roche et al. (code by E. Haug, Rad. Phys. Chem. 77 (2008) 207).

Measurement of the electron energy via photodisintegration of deuterons

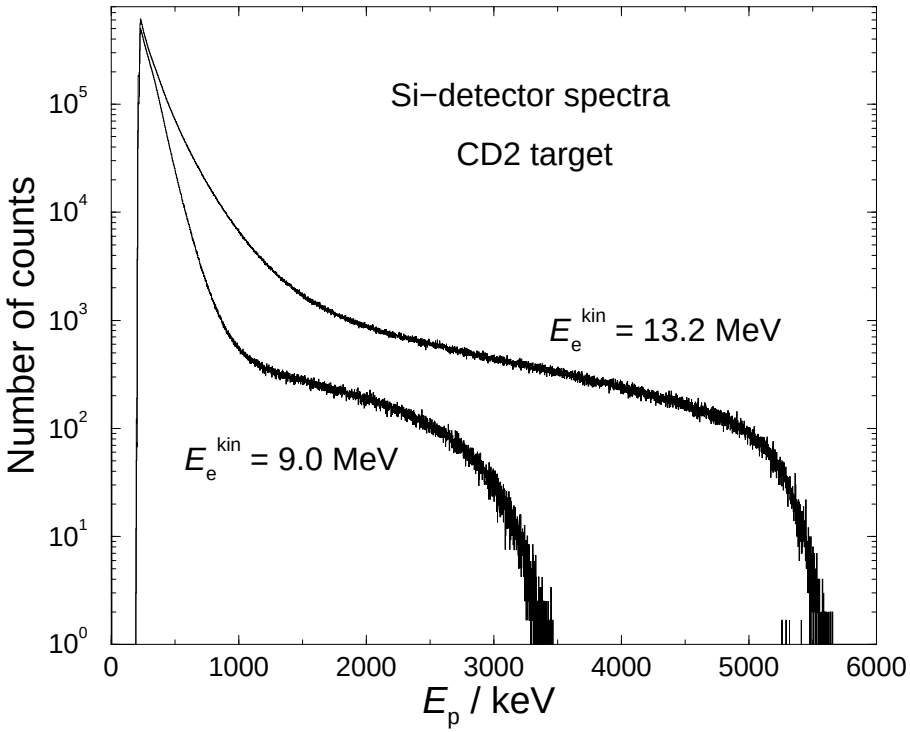

Spectra measured with Si detectors of 300 μm thickness during the irradiation of a deuterated polyethylene film with bremsstrahlung.

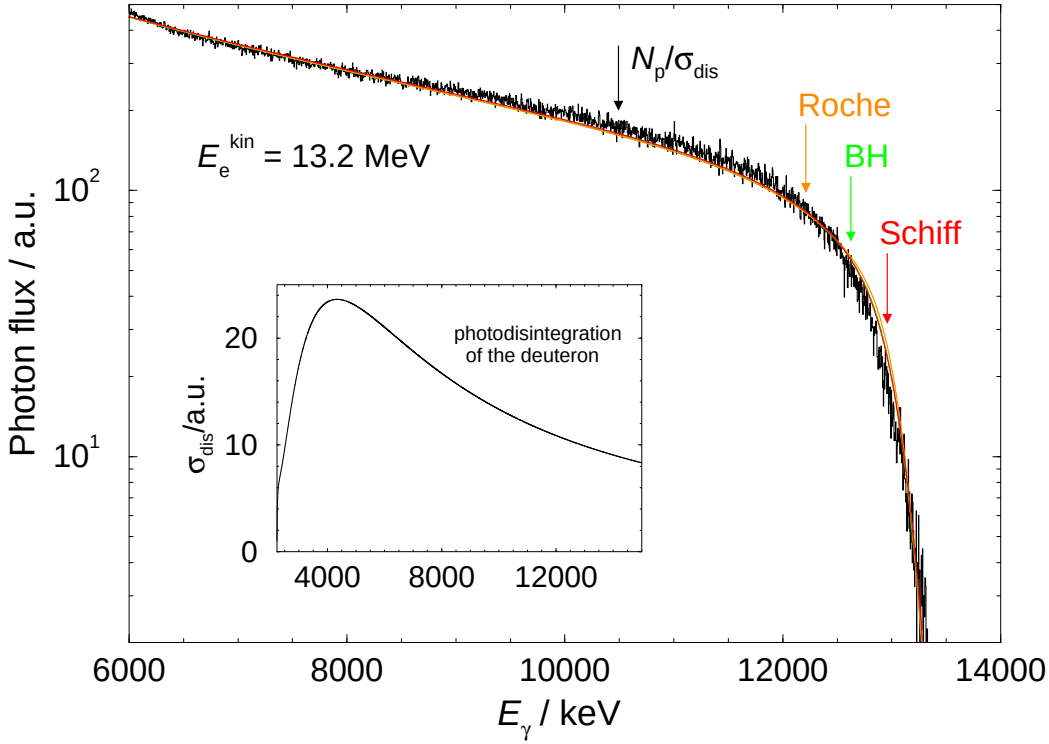

Spectrum of incident photons recalculated from the proton spectrum and the cross section for the disintegration of the deuteron.

σ_{dis}: H. Bethe, C. Longmire, Phys. Rev. 77 (1950) 647
Roche: G. Roche *et al.*, Phys. Rev. A 5 (1972) 2403
BH: H. Bethe, W. Heitler, Proc. Roy. Soc. A 146 (1934) 83
Schiff: L.I. Schiff, Phys. Rev. 83 (1951) 252